Optimisation of Interior Permanent Magnet Generator in Propeller Type Tidal Turbines
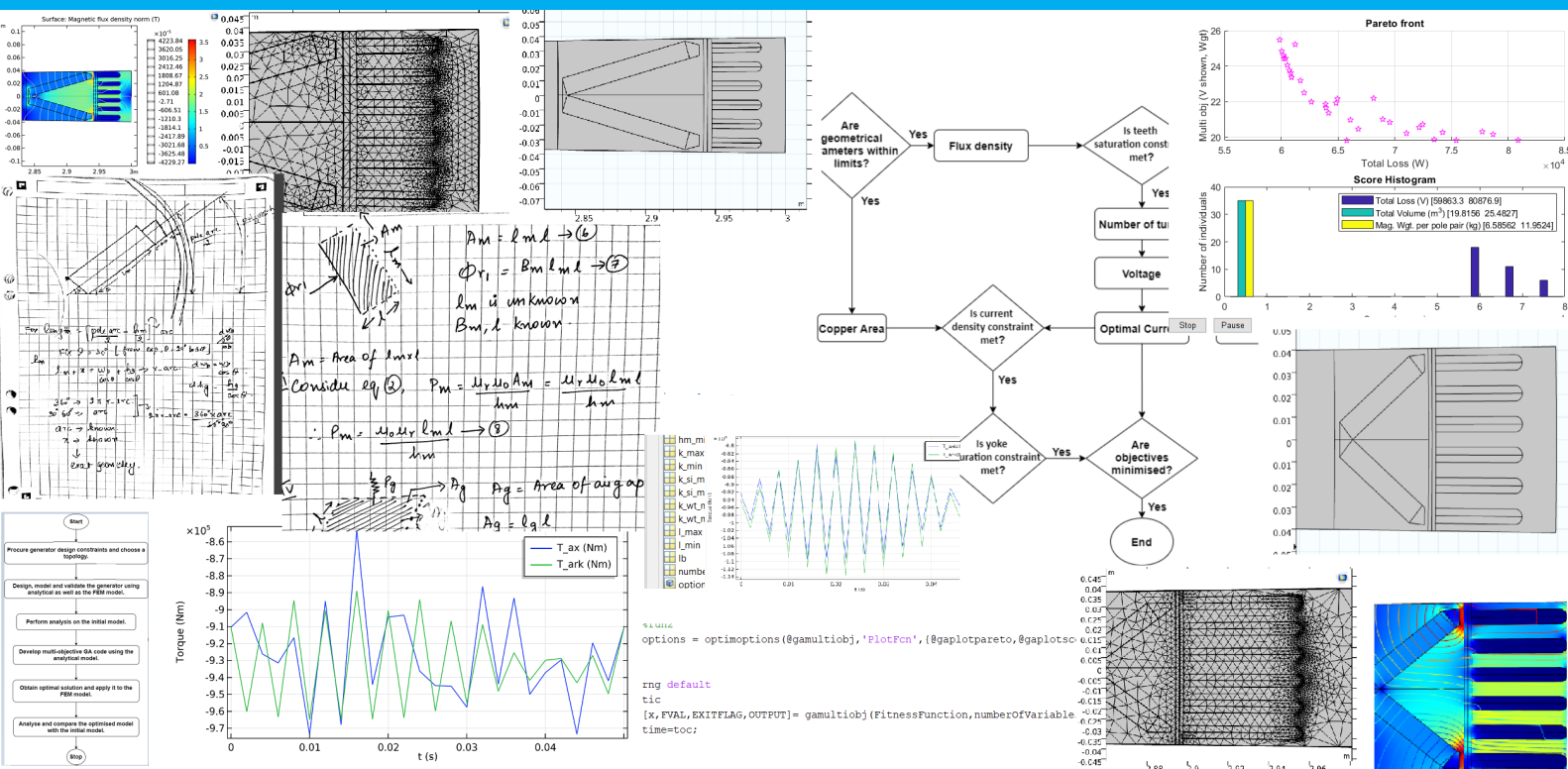
Devika B S

(Bindhu Sreevalsan, Devika)

TUDelft

Optimisation of Interior Permanent Magnet Generator in Propeller Type Tidal Turbines

by

Devika Bindhu Sreevalsan

to obtain the degree of Master of Science
at the Delft University of Technology,
to be defended publicly on Wednesday February 3, 2021 at 9:00 AM.

An electronic version of this thesis is available at `http://repository.tudelft.nl/`.

TUDelft

Abstract

Over the past few decades, there has been a steep increase in efforts to generate electricity from clean and renewable energy sources so as to reduce consumption of fossil fuels. A considerable amount of research is in progress to explore the scope of various sustainable power sources; among which tidal energy is estimated to have a huge potential. With advancements in technology, it is predicted that electricity from tidal energy would increase in the coming years. It is necessary to have highly efficient generators that can convert tidal energy to electricity. Propeller type generation system using Permanent Magnet Synchronous Machines (PMSMs) are found to be suitable for the application of tidal generators. For the best utilisation of resources, it is essential to improve the performance of these machines in several aspects. And hence, multi-objective optimisation of electrical machines is emerging to be of high significance.

The key goal of this thesis is to design, model and optimise a PMSM generator so as to get the desired power while considering other design objectives, including the efficiency, total volume of the machine and weight of magnets.

The thesis is divided into two parts. The first part consists of design, modelling and analysis of the PMSM machine. Initially, all the required machine constraints are identified and a topology is selected. An analytical model is built after which the machine is modelled using the Finite Element Method (FEM). The model is analysed where various key characteristics of the machine such as flux linkages, induced EMF, inductance and torque are calculated. This is validated by ensuring that results from FEM model and analytical model match. In order to optimize the machine; certain geometric parameters are varied to locate the dominant geometrical parameters.

The second part of the machine consists of optimisation. A multi-objective Genetic Algorithm (GA) optimization is carried out to generate data to search for an optimal design. The three objectives for optimisation are higher efficiency, lower total volume and lesser weight of magnets. The analytical model is used in the optimisation algorithm. Since this is a multi-objective optimisation, a set of solutions (Pareto set) is generated from which a single solution is chosen. This selected solution is applied to the FEM model and thus finally an optimized model of the machine is developed. An analysis is carried out on the optimised model. Finally, the optimised model and the initial model are compared and the results are explained.

Preface

I thank my supervisor Dr. Jianning Dong for his feedback and technical guidance during the course of the project; as well as other thesis committee members Dr. Pavol Bauer and Dr. Domenico Lahaye for their valuable inputs.

I would like to express my deep gratitude to some of my friends at Delft, especially that of Adithya for his help during some hard times of my stay in the Netherlands.

I thank my parents for their constant love and support.

Devika Bindhu Sreevalsan
Delft, January 2021

Contents

List of Figures

List of Tables

Nomenclature

List of abbreviations

PTO-Power Take-Off

TiPA-Tidal Turbine Power Take-Off Accelerator

IEA-International Energy Agency

PM-Permanent Magnet

PMSM-Permanent Magnet Synchronous Machine

GW-gigawatt

GA-Genetic Algorithm

PSO-Particle Swarm Optimisation

IPM-Interior Permanent Magnet

FEM-Finite Element Method

EMF-Electromotive force

DC-Direct Current

RMS-Root Mean Square

MTPA-Maximum Torque Per Ampere

List of Symbols

l - Axial length of the machine [m]

h_g - Geometrical length of air gap [m]

S - Tangential stress of the machine [Pa]

k_{car} - Carter factor [-]

D - Stator inner diameter [m]

τ_s - Slot pitch [m]

τ_p - Pole pitch [m]

h_{gc} - Length of modified air gap after including Carter factor [m]

B_g - Magnitude of assumed flux density at air gap [T]

B_{g1-fun} - Fundamental component of assumed flux density at air gap [T]

l_m - Length of magnet [m]

h_m - Width of magnet [m]

w_b - Length of magnetic bridge [m]

k_{si} - Ratio of stator inner radius to stator outer radius [-]

k_{wt} - Ratio of slot teeth to slot pitch [-]

α - Ratio of pole arc to pole pitch [-]

θ_{mag} - Angle between the two magnets [°]

θ_{main} - Angle of the main sector containing a pole [°]

ϕ_{r1} - Remanent flux of magnet [Wb]

ϕ_{pp} - Flux per pole [Wb]

P_m - Permeance of magnet [H]

P_g - Permeance of air gap [H]

B_{sat} - Magnetic flux density of the bridge [T]

B_m - Magnetic flux density of the magnet [T]

B_r - Radial component of flux density at the air gap [T]

B_θ - Tangential component of flux density at the air gap [T]

μ_0 - Permeability of free space [H/m]

μ_r - Relative permeability of magnetic material [-]

N_{slots} - Total number of stator slots in a machine [-]

N_{phase} - Number of phases [-]

q - Slots per pole per phase [-]

N_{series} - Number of series turns in a phase [-]

E_{ph-rms} - RMS value of induced EMF in a phase [V]

I_{ph-rms} - RMS value of current in a phase [A]

K_w - Winding factor [-]

z_{qtotal} - Total number of conductors [-]

z_q - Number of conductors in a slot [-]

n_{pp} - Number of parallel paths [-]

I_{slot} - Current flowing through a slot [A]

Ar_{Cu} - Area of Copper [m^2]

Ar_{slot} - Area of slot [m^2]

K_{fill} - Fill factor [-]

R_{AC} - AC resistance of phase winding [Ω]

k_R - Skin effect factor [-]

l_{av} - Average length of a turn [m]

W - Coil span [m]

y_{thick} - Thickness of yoke [m]

d_s - Slot depth [m]

V_{yoke} - Volume of yoke [m^3]

V_{teeth} - Volume of teeth [m^3]

P_{mech} - Mechanical power generated by the machine [W]

P_{cu} - Copper loss [W]

P_{iron} - Iron loss [W]

$P_{Fe_{yoke}}$ - Iron loss at yoke[W]

$P_{Fe_{teeth}}$ - Iron loss at teeth[W]

$T_{Mstress}$ - Torque calculated from Maxwell's stress tensor method [Nm]

T_{ark} - Torque calculated from Arkkio's method [Nm]

w_s - Width of slot [m]

w_t - Width of teeth [m]

k_{Fe_y} - Correction coefficient of iron loss at yoke [-]

k_{Fe_t} - Correction coefficient of iron loss at teeth [-]

m_{yoke} - Mass of yoke [kg]

m_{teeth} - Mass of teeth [kg]

$\rho_{Si_{steel}}$ - Density of Silicon steel [kg/m^3]

ρ_{mag} - Density of magnet [kg/m^3]

θ_e- Electrical angular displacement [rad]

θ_m- Mechanical angular displacement [rad]

n_s- Synchronous speed of machine [RPM]

ω_e- Electrical angular speed [rad/s]

ω_m-Mechanical angular speed [rad/s]

$\vec{B}$ - Magnetic flux density [T]

$\vec{H}$ - Magnetic field intensity [A/m]

$\vec{E}$ - Electric field intensity [V/m]

$\vec{J}$ - current density [A/m^2]

λ_d- Magnetic Flux linkages along d axis [Wb]

λ_q= Magnetic Flux linkages along q axis [Wb]

I_q-Current along q axis [A]

I_d-Current along d axis [A]

L_q-Inductance along q axis [H]

L_d-Inductance along d axis [H]

f_{elec} - Electrical frequency [Hz]

T_{elec} - Electrical time period [s]

T_{em} - Electromagnetic torque [Nm]

T_{ex} - Excitation torque [Nm]

T_{rel} - Reluctance torque [Nm]

T_{emu} - Per unit value of T_{em} [-]

T_{relu} - Per unit value of T_{rel} [-]

i_{su} - Per unit value of i_s [-]

i_{du} - Per unit value of i_d [-]

i_{qu} - Per unit value of i_q [-]

1

Introduction

1.1. Background

Over the past couple of decades, there has been an increase in demand for electricity from renewable energy sources considering the depletion of fossil fuels as well as the adverse environmental impacts caused due to the consumption of fossil fuel.
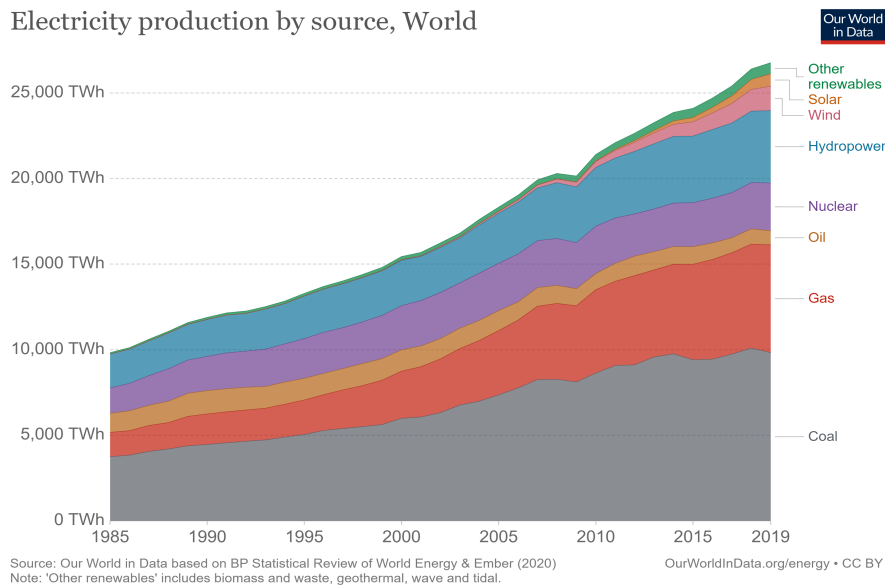
Figure 1.1: Electricity production by source [8].

As seen in fig.1.1, though coal continues to be the primary source of fuel, the percentage of energy from renewable energy sources have been steadily increasing [8].

Tidal energy is a form of renewable energy that uses tidal action in oceans to generate electricity. Tidal action occurs due to the difference in water levels between high tide and low tide which in turn is because of the gravitational pull of moon on the earth's surface [46].

An innovative technology called direct drive Power Take-Off (PTO) is currently under research. This is more efficient and requires less maintenance compared to conventional PTO because it does not need a gear box [41]. The illustration of both conventional PTO and direct drive PTO is shown in fig.1.2. The generator in this thesis is suitable for the direct drive PTO.

The advantages of tidal power are [18]:

- **Predictable**
  Tidal energy is predictable. There are no uncertainties regarding the availability of tidal energy at a given source.

1
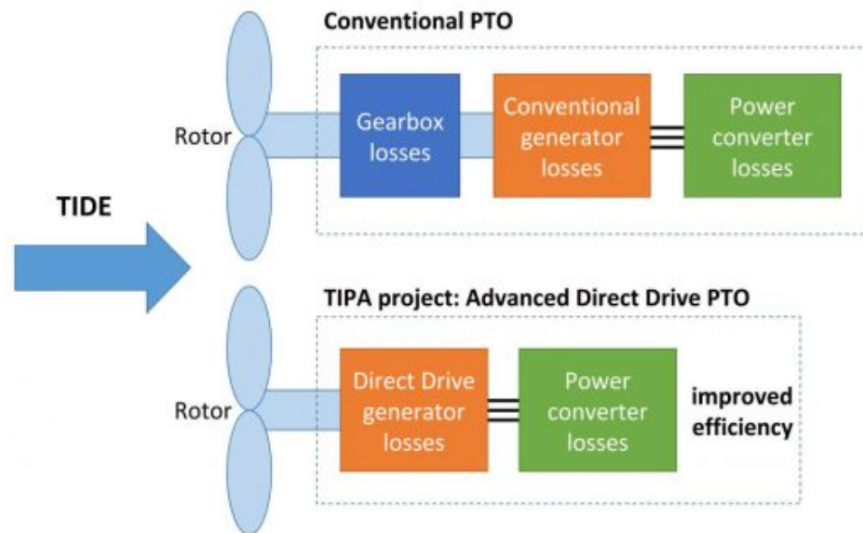
Figure 1.2: Flow Chart of Tidal Energy Conversion, conventional PTO vs. direct drive PTO [41].

- **Clean and renewable**
  Tidal energy is a clean and renewable energy source in contrast to energy supply coming from fossil fuels. Unlike fossil fuels, tidal energy sources emit zero green house gases.

- **Longevity of Power plants**
  Since tidal power plants primarily consist of tidal barrages made of concrete structures, these power plants last relatively much more longer than wind and solar power plants.

The disadvantages of tidal power are [18]:

- **Expensive to construct**
  Tidal power plants have very high costs of construction.

- **Impact of electromagnetic emissions**
  Many marine life species use natural magnetic field for navigation. Electromagnetic emissions from tidal power plants may disrupt the natural magnetic field thus adversely affecting marine life. There is a lack of research regarding the environmental impacts of tidal energy.

Head Classification	Turbine Type		
	Impulse	*Reaction*	*Gravity*
High (>50m)	• Pelton • Turgo		
Medium (10-50m)	• Crossflow • Turgo • Multi-jet Pelton	• Francis (spiral case)	
Low (<10m)	• Crossflow • Undershot waterwheel	• Propeller • Kaplan • Francis (open-flume)	• Overshot waterwheel • Archimedes Screw

Figure 1.3: Classification of turbines [19].

Presently, tidal energy technology is at an early phase of development. However, International Energy Agency (IEA) forecasts that by 2050 wave and tidal power could reach a capacity of more than

330(GW) globally [1].

Propeller type turbine is a reaction turbine suitable for low head applications.
In a reaction turbine, the rotor is completely submerged in the fluid. Similar to how blades in a flight experience lift, it is the pressure difference across the blades in a propeller turbine that results in the lift force [19]. The classification of turbines is shown in fig.1.3.

1.1.1. Selection of generator

The most commonly used generators in tidal turbines are squirrel cage induction machines and Permanent Magnet Synchronous Machines (PMSM). Despite being expensive, PMSM are chosen among synchronous machines because of its low failure rate and possibility of having large number of poles [55].
In PMSM, flux linkage is created by permanent magnets instead of field windings. Fig.1.4 is a diagram showing a PMSM [42].
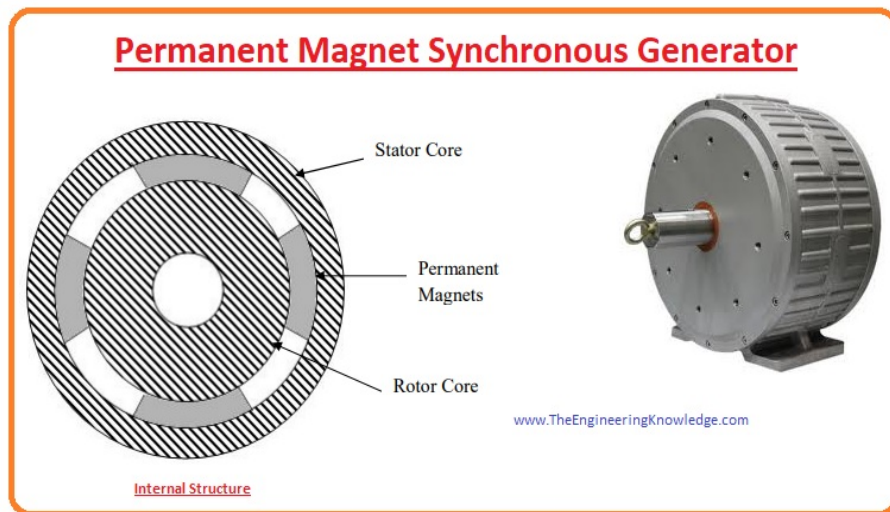
Figure 1.4: PMSM [5].

Since PMSM have no excitation losses, they are inherently more efficient. But like most machines, Joule losses occur in PMSMs as well. PMSMs are suitable for low speed high torque applications. This is because at low speeds, losses in magnets remain low [42].

The characteristics of PMSMs depend entirely upon the construction of the machine. Different types of rotor PMSM constructions are illustrated in fig.1.5. The rotor construction can be classified as surface mounted magnets and embedded magnets.
Surface mounted magnets are non salient because the relative permeability of neodymium–iron–boron magnets is close to one [53]. Around 5-10% of the flux is lost as leakage in magnet edge areas. The permanent magnet is best used when it is surface mounted. This is because these machines produce the highest pull-out torque since the synchronous inductance is low which is a consequence of high magnetic circuit reluctance. The main disadvantages of this type of construction is it vulnerable to eddy current loss and mechanical stress. Additionally, there is a possibility of the magnets getting demagnetised [42].
In embedded magnets, the quadrature axis inductance is higher than the direct axis inductance. When the magnets are embedded, typically one forth of the flux is wasted and this flux is consumed by leakage components of the rotor [42]. The leakage can be reduced by using a flux barrier of air as shown in fig.1.6. Embedded magnets have the advantages of being protected both mechanically as well magnetically.
fig.1.5.
Since in IPMSM, the magnets are embedded inside the rotor core; it prevents separation of PM from centrifugal force at high speeds and also generates a hybrid torque consisting of electromagnetic
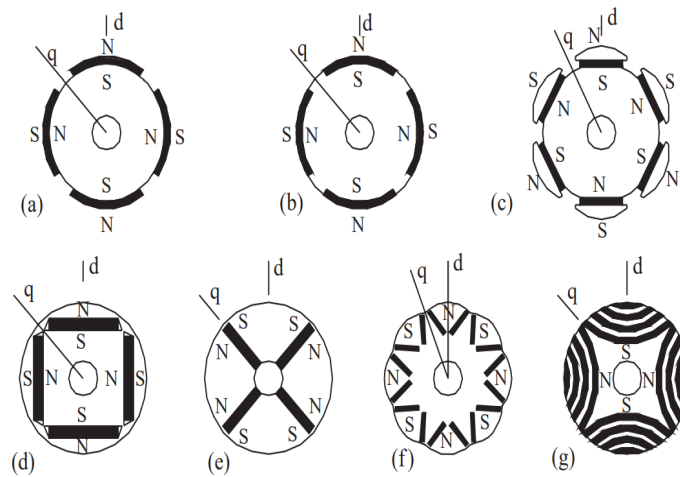
Rotors of permanent magnet machines. (a) Rotor-surface-mounted magnets, (b) magnets embedded in the surface, (c) pole shoe rotor, (d) tangentially embedded magnets, (e) radially embedded magnets, (f) two magnets per pole in the V position, (g) a synchronous reluctance rotor equipped with permanent magnets. Reproduced by permission of Tanja Hedberg, based on Morimoto, Sanada and Taniguchi (1994)

Figure 1.5: Different types of rotor construction [42].
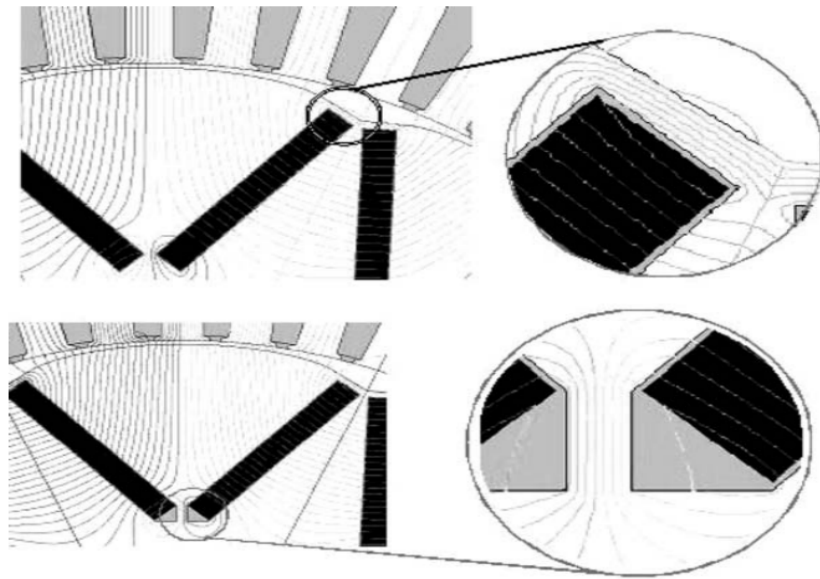
Figure 1.6: Reduction of leakage using air barrier in embedded 'V' type magnet [42].

torque, reluctance torque as well as cogging torque. The interaction of stator currents and rotor PMs produce electromagnetic torque. The rotor saliency creates reluctance torque. Interaction between slotted teeth structure and PMs cause cogging torque [30].

Among embedded magnet PMSM there are several rotor configurations - each having its own advantages and disadvantages. Both 'V' type and spoke magnets have lower torque ripple at higher values of current [21]. However spoke type magnets have higher iron losses compared to 'V' type magnets [21]. Another advantage of using 'V' type magnet is that in this type of construction where there are two magnets per pole, under no-load conditions; it is possible to attain a high value of air gap flux density [42]. Considering all these aspects, 'V' type magnet was chosen for the design.

Finally, propeller type generation system with PMSM that uses embedded 'V' shaped magnets is used

in this thesis.

Selection of the final topology

From the choices made so far, it is seen that the generator suitable for this application is a PMSM with embedded 'V' type magnets. Based on this and existing research, the topology in fig.1.7 was fixed.
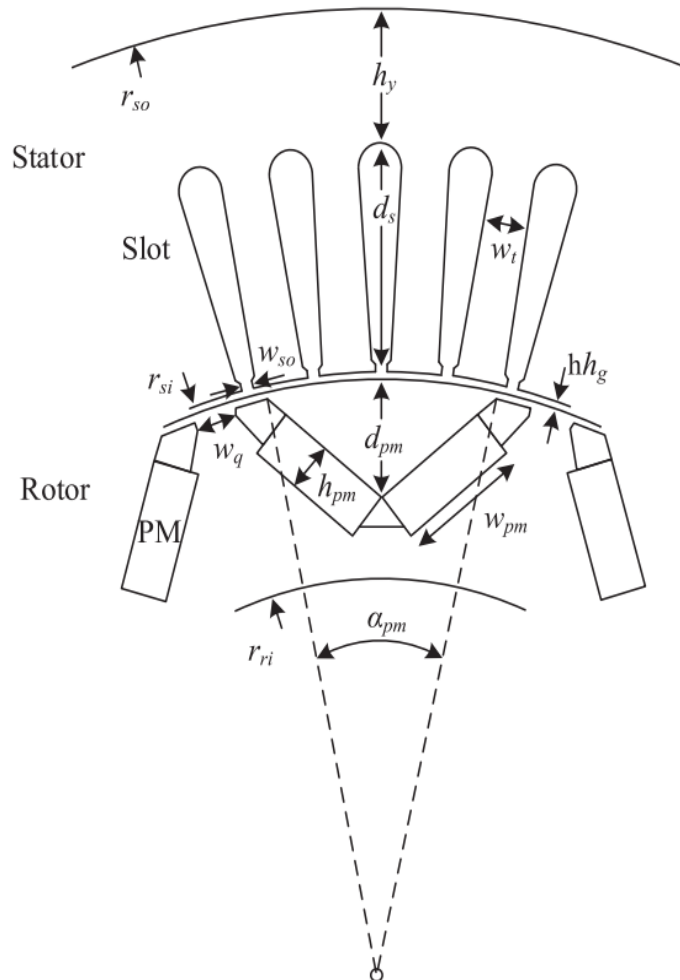
Figure 1.7: Final topology chosen [13]

Basically fig.1.7 is the geometry of a generic industrial Interior Permanent Magnet (IPM) motor [13]. In this thesis, the same topology with minor alterations at the slot opening and flux barriers will be used. Flux barriers are the air barrier places at the end of magnets to shape the magnetic field at the rotor poles. The magnet material is the main parameter that affects the shape of flux barrier [45]. The shape of this flux barrier can affect average steady torque, torque ripple and cogging torque [20].

1.2. Research Focus

The core research focus of this thesis is the design, modelling and optimisation of Permanent Magnet synchronous generator for the application of tidal generators. The main focus when it comes to the design and modelling of machine is the selection of machine according to its suitability for a tidal generator. Next the choice of performance factors for optimisation are explored. Since this is a tidal generator, the machine is huge and hence minimising volume is an optimisation objective. In case of embedded magnets, there is leakage of flux linkages. Also 'V' shape magnets need more magnet mass. So, reduction of magnet weight is another objective to optimise. Optimising the first two performance factors must not adversely affect the total efficiency of the machine. So, the third objective is

maximising the total efficiency of the selected machine. Then the focus shifts to identifying the design parameters that would contribute to the final performance factors from the initial model. This is followed by the selection of the right optimisation algorithm for this thesis. Finally, the question of a trade-off between conflicting objectives are addressed.

1.2.1. Research Questions
The research questions addressed during the thesis are

- What type of electrical machines are suitable for tidal generators?

- What are the main performance factors to optimise?

- Which design parameters influence machine performance the most?

- How to select a suitable optimisation algorithm?

- Among the chosen multi-objectives, how is the trade-off between conflicting objectives made?

1.2.2. Objectives of the thesis
- To design, model and analyse a PMSM generator.

- To perform a multi-objective optimisation on the initial model.

- Apply the optimised solution and analyse the optimised machine.

- Compare the optimised model with the initial model and explain the results.

1.3. Flow Chart of Thesis
The flow chart of the thesis is given in fig.1.8.

- **Procure generator design constraints and choose a topology.**
  First the generator design constraints are obtained. After which a suitable topology is chosen.

- **Design, model and validate the generator using analytical as well as the FEM model.**
  The generator is designed such that it satisfies the initial constraints. Both models - an analytical as well as Finite Element Method (FEM) model are developed. The models are then checked for errors and corrected in case errors are found.

- **Perform analysis on the initial model.**
  Various calculations are performed on the model to check the performance - such as the flux density produced at the air gap, flux linkages, induced EMF, inductance, optimal current and the torque produced.

- **Develop multi-objective GA code using the analytical model**
  To optimise the existing parameters, a multi-objective Genetic Algorithm (GA) code is developed. Before that based on the analysis of the initial model, the parameters that are to be optimised have to be identified. After this, the analytical model is used for optimisation. This is because using the FEM model directly would result in a large amount of time for running the optimisation code for IPM synchronous machines [16].

- **Obtain optimal solution and apply it to the FEM model**
  Since a multi-objective GA code is run, a Pareto set containing a lot of solutions would be obtained. Using a trade off, a particular solution has to be selected from the Pareto set and then applied to the FEM model.

- **Analyse and compare the optimised model with the initial model.**
  Once again, various calculations are performed on the model to check the performance - such as the flux density produced at the air gap, induced EMF, inductance, optimal current and the torque produced. After this, both the initial model as well as the optimised model are compared and the results are explained.

Software Used: The FEM model is modelled using COMSOL Multiphysics. The analysis is done using both COMSOL Multiphysics as well as MATLAB with LiveLink to interface between them.
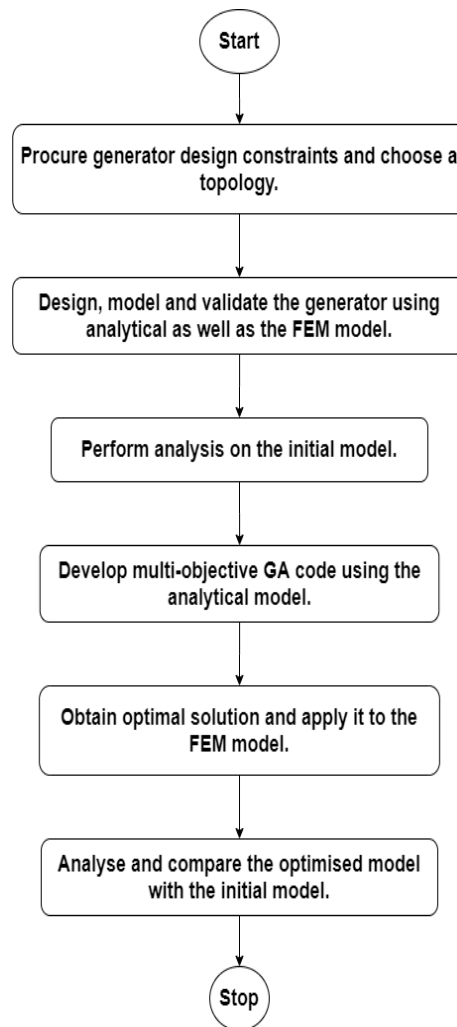
Figure 1.8: Flow chart of the Thesis

1.3.1. Report Structure

Chapter 1 consists of introduction to the thesis where the background, research and structure of the thesis is written. Chapter 2 comprises of the theory and design methodology used in this thesis. Concepts and equations behind the analytical model, FEM model and optimisation techniques are discussed in detail. Chapter 3 contains the design and analysis of the initial model. Chapter 4 consists of the multi-objective GA flow chart and Pareto solutions. In chapter 5, the analysis of optimised model is explained in detail. And finally, the results of this thesis are summarised where both the initial and optimised models are compared followed by chapter 6 that contains conclusions and recommendations.

2

Theory and Design Methodology

2.1. Analytical Modelling of the Machine

One of the first steps in design of machine is to find the main dimensions - the axial length (l) and the air gap length (h_g)

2.1.1. Sizing of the machine

The tangential stress (S) of the machine is a starting point for determining the main dimensions of a machine. Tangential stress is the force density that generates torque. Once torque and tangential stress are determined, then the main dimensions can be obtained. The value of S can be selected from a standard table which is created based on the insulation and cooling of the machine [42]. From the reference in fig.2.1, the value of S was selected to be 33,500 Pa which is the average value

Tangential stresses $\sigma_{F\text{tan}}$ calculated from the values of Tables 6.1 and 6.2. There are three stress values, calculated with the lowest linear current density and flux density, with the average values and with the highest values. The flux density and linear current density distributions are assumed sinusoidal. For DC machines, a pole width coefficient of 2/3 is assumed. The power factor of synchronous machines is assumed to be 1, and for asynchronous machines, 0.8

	Totally enclosed asynchronous machines	Sailent-pole synchronous machines or PMSMs	Nonsalient-pole synchronous machines			DC machines
			Indirect cooling		Direct water cooling	
			Air	Hydrogen		
A/kA/m, RMS	30–65	35–65	30–80	90–110	150–200	25–65
Air-gap flux density $\hat{B}_{\delta1}$/T	0.7–0.9	0.85–1.05	0.8–1.05	0.8–1.05	0.8–1.05	0.6–1.1
Tangential stress $\sigma_{F\text{tan}}$/Pa						
minimum	12 000*	21 000*	17 000*	51 000*	85 000*	12 000*
average	21 500*	33 500*	36 000*	65 500*	1,14 500*	29 000*
maximum	33 000*	48 000*	59 500*	81 500*	1,48 500*	47 500*
	*$\cos\varphi = 0.8$	*$\cos\varphi = 1$	*$\cos\varphi = 1$	*$\cos\varphi = 1$	*$\cos\varphi = 1$	*$\alpha_{DC} = 2/3$

Figure 2.1: Standard values of tangential stress for different machines [42].

of tangential stress in a PMSM machine.

Next from the Sizing Equation [42]

$$l = \frac{2T_{mech}}{S\pi D^2}$$

(2.1)

where D is the stator inner diameter.

Determining Air Gap Length
The air gap length has a significant influence on the characteristics of a machine. A small air gap gives a low magnetising current. However, harmonics present in open or semi open slots can give rise to eddy current losses. A small air gap can give rise to more surface losses in rotor which is a consequence of current linkages harmonics in the stator. Technically the smallest possible air gap is around 0.2 mm. Though the air gap is of great significance with respect to the harmonics in a machine, as of now a theoretical formula that can calculate the optimum dimension of an air gap has not yet been developed. However, some empirical equations are used to find the length of an air gap based on the size of the machine [42].

Since this is a tidal generator, the machine is considered to be 'exceptionally large'. The formula used to calculate the dimension of such machines is [42]:

$$h_g = 0.001 * 2 * r_{si} \tag{2.2}$$

Carter factor
Carter factor is used to simplify the geometry around the air gap. As shown in fig.2.2, in electrical machines the flux density decreases at the region of slot opening. This implies that the air gap appears to be longer than its actual physical dimension. To incorporate this into the model, a correction factor called 'Carter factor' (k_{car}) is included in the air gap dimension [42].
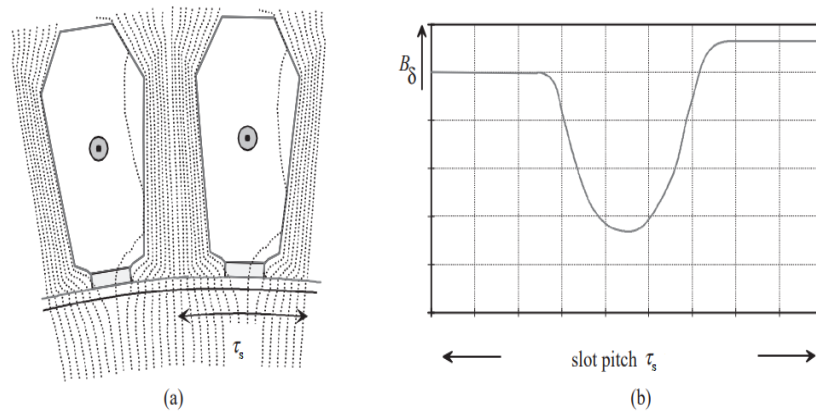
(a) Flux diagram under a stator slot along one slot pitch, and (b) the behaviour of the air-gap flux density B_δ along a slot pitch. At the slot opening, there is a local minimum of flux density. The flux density on the right side of the slot is slightly higher than on the left side, since a small current is flowing in the slot towards the observer

Figure 2.2: Decrease of flux density at slot opening [42]

.

In order to calculate the Carter factor, a rectangular function is used instead of the actual flux density. When using the rectangular function, flux remains constant under the teeth and zero at the slot opening [42].

The modified air gap dimension using Carter factor is not exact but has sufficient accuracy. To obtain even higher accuracy, the field diagram of the field diagram of the air gap has to be solved using the finite element method. However, in this thesis; Carter factor is used.

Below are the equations used to determine k_{car} [42]:

$$h_{gc} = k_{car} h_g \tag{2.3}$$

$$k_{car} = \frac{\tau_s}{\tau_s - b_e} \tag{2.4}$$

$$b_e = k_{pc} w_s \tag{2.5}$$

$$k_{pc} = \frac{2}{\pi}[arctan\frac{w_s}{2h_g} - \frac{2h_g}{w_s}ln\sqrt{1 + (\frac{w_s}{2h_g})^2}] \tag{2.6}$$

τ_s= slot pitch, w_s=slot width,
h_g=original air gap, h_{gc} = modified air gap
Flux density at air gap
The air gap flux density is assumed to be trapezoidal in shape as shown in fig.2.3. The fundamental component of the air gap flux density is calculated using Fourier series.
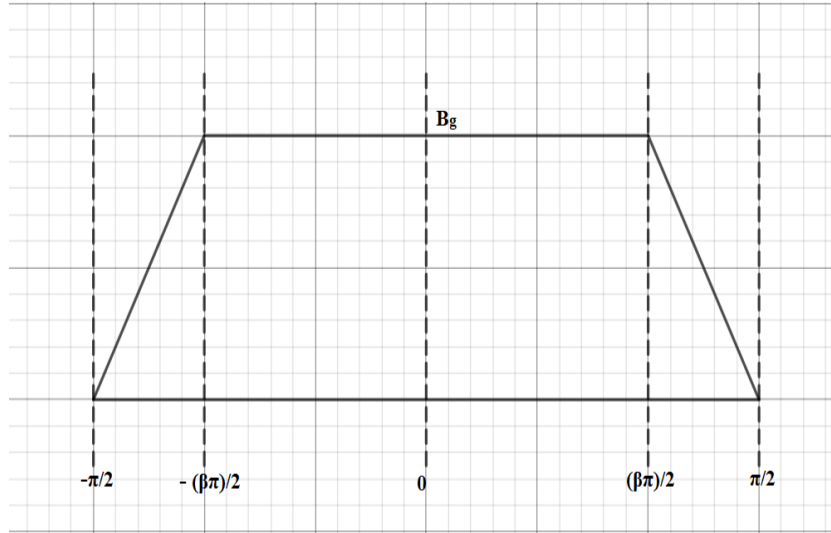
Figure 2.3: (Assumed) Trapezoidal flux density at air gap

$$Bg_{1-fun} = \frac{4}{\pi}Bg\, sin[\frac{(\frac{\pi-\beta\pi}{2})}{(\frac{\pi-\beta\pi}{2})}] \tag{2.7}$$

2.1.2. Rotor Design: The Magnetic Circuit
The main purpose of using the magnetic circuit in this thesis is to find a mathematical expression that relates the flux per pole to the geometry of the rotor magnet.
In case of the reverse model, solution of the magnetic circuit would be obtaining the length and breadth of a magnet for a given flux per pole - i.e. the geometry is not fixed first. Whereas in case of the forward model, solution of the magnetic circuit will determine whether the geometry, (length and breadth of magnet) will produce the required flux per pole - i.e, the geometry is fixed first and then the algorithm is designed such that it checks whether the geometry will produce the required flux per pole.
The magnetic circuit of a V shaped magnet is given in fig.2.4.
In the thesis, the V shape magnets touch each other and hence the magnetic circuit from above is slightly modified such that w_c = 0.
Also, the variable l_m from the figure is renamed as h_m which is the width of the magnet, h_g is used instead of g for the air gap length, w_b is the magnetic bridge length.

The equations to solve the magnetic circuit are given as follows [24]:

$$\phi_{pp} = (2\phi_{r1} - 2\phi_{b1})(\frac{P_g}{2P_m + P_g}) \tag{2.8}$$

Where ϕ_{pp} is the flux per pole
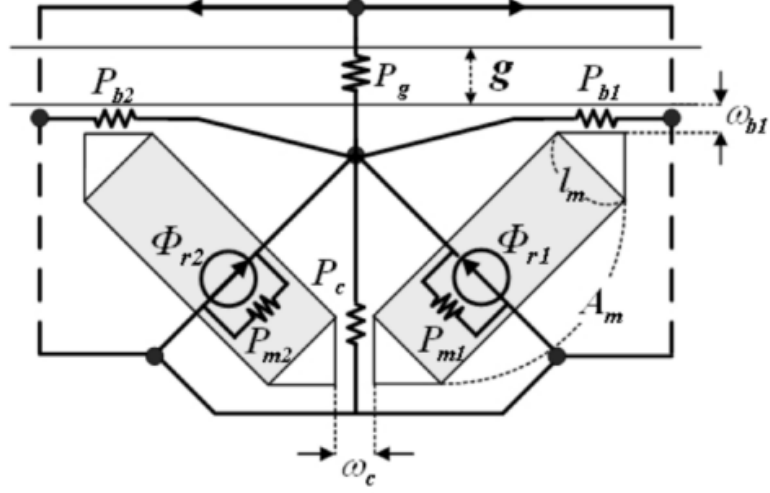
Figure 2.4: The Magnetic Circuit [24].

$$P_{m1} = P_{m2} = P_m = \frac{\mu_r \mu_0 A_m}{h_m} \tag{2.9}$$

$$P_g = \frac{\mu_0 A_g}{h_{gc}} \tag{2.10}$$

$$\phi_{b1} = \phi_{b2} = \phi_b = B_{sat} * w_b * l \tag{2.11}$$

Where l is the axial length of the machine.
The length of the magnetic bridge is assumed to be half of that of the air gap. This is a starting value for this dimension. The magnetic bridge is assumed to be saturated. And hence a narrow value is chosen for this dimension.

$$w_b = \frac{h_{gc}}{2} \tag{2.12}$$

Since the magnetic bridge is narrow and assumed to be saturated,

$$\Phi_b = B_{sat} w_b l \tag{2.13}$$

where Φ_b is the flux through the bridge, B_{sat} is the saturation flux density.
Similiarly,

$$\Phi_{r1} = B_m A_m \tag{2.14}$$

$$A_m = l_m l \tag{2.15}$$

Where l_m is the length of the magnet. The permeance of the magnet is calculated as:

$$P_m = \frac{\mu_0 \mu_r l_m l}{h_m} \tag{2.16}$$

$$A_g = l_g l \tag{2.17}$$

l_g is the length of the main sector of rotor that contains a single pole of the V magnet as illustrated using the $l_g l$ plane in fig.2.5.

The dimension of l_g is obtained as:
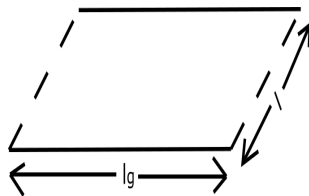
Figure 2.5: Plane $l_g l$

$$l_g = \frac{2\pi r_{si}\frac{\theta_{main}}{2}}{360} \tag{2.18}$$

where θ_{main} is the angle of the main sector of rotor.
The permeance of the air gap P_g is calculates as:

$$P_g = \frac{\mu_0 l_g}{h_{gc}} \tag{2.19}$$

Finally, the flux per pole is obtained

$$\Phi_{pp} = \frac{(2\Phi_{r1} - 2\Phi_{b1})P_g}{2P_m + P_g} \tag{2.20}$$

$$l_m = kh_m \tag{2.21}$$

k is the ratio of length to breadth of the magnet.
Solving the magnetic circuit gives the dimensions of the magnet.

$$h_m = \frac{\frac{\phi_{pp}(k_2+w)}{w} + k_1}{k_4} \tag{2.22}$$

The width of the magnet is determined first.

$$l_m = kh_m \tag{2.23}$$

Then the length of the magnet is obtained.
where

$$k_1 = 2B_{sat}w_b l \tag{2.24}$$

$$k_2 = 2P_m \tag{2.25}$$

$$k_3 = \frac{\mu_0 l}{h_{gc}} \tag{2.26}$$

$$k_4 = 2B_m kl \tag{2.27}$$

$$w = k_3 l_g \tag{2.28}$$

In case of using the magnetic circuit in the forward model, the equations remain the same. The order of using them during the optimisation part changes. First the geometry - the dimensions of the magnet are fixed and then the program calculates the flux per pole.

2.1.3. Stator Design: Design of Winding

The first step in stator design is the design of winding. In winding design, the main decisive factors are the total number of slots, the number of slots per pole and type of winding - concentrated or distributed winding. The selection of these factors entirely depends upon the application and required performance. In case of concentrated winding, the voltages induced in the coil are in phase and hence the voltages of the windings is the arithmetic sum of individual coil voltages. This in in contrast with distributed windings where the coils belonging to a winding are distributed over several slots in space. Distributed windings make better use of stator structure and reduce harmonics [47].

The selection of the total number of slots depends upon the geometry of the slot width. If there are too many slots, then the slot width would be too narrow and if the number of slots is too less, then the slot width would be very wide. Since this is a three-phase machine where each turn consists of two conductors, the number of slots should also be a multiple of 3*2 (6). Else there would be an unbalance of magnetic pulling forces in the air gap which will no longer be symmetric.

Next comes the choice of integral slot winding or fractional slot winding. The slots per pole per phase (q) can be calculated as below where N_{slots} is the total number of slots and N_{phase} is the number of phases [42]

$$q = N_{slots}/(P * N_{phase}) \tag{2.29}$$

When q is an integer, the winding is called an integral slot winding. When q is a fraction greater than 1, the winding is a fractional slot winding. For a fractional slot concentrated winding, q is a fraction less than 1. The choice of q determines winding factor as well as winding harmonics. An increase in value of q would lead to a decrease of the fundamental winding factor [2].

From a comparative study of performance of PMSM for both fractional as well as integral slot winding, it was observed that fractional slot windings have lesser cogging torque and torque ripple. But this comes with a disadvantage of reduction of average torque and unbalanced radial magnetic forces [15]. Additionally, in case of sinusoidal current distribution, use of fractional number of slots per pole was found to increase harmonics content of magnetic vector potential and normal component of the magnetic flux density waveforms [15].

In this thesis, the objectives of optimisation do not include reduction of cogging torque or torque ripple. And hence, it is not required to use fractional slot winding. Integral slot winding is more suitable.

2.1.4. Stator Design: Finding number of parallel paths and slot area

Finding the number of parallel paths

The procedure to find the number of parallel paths is [42] [44]:

First from equation of induced EMF in a 3 Phase synchronous machine, N_{series} is calculated.

Equation of induced EMF in a 3 Phase synchronous machine is given by:

$$E_{ph-rms} = 4.44 f \phi_{pp} N_{series} K_w \tag{2.30}$$

where E_{ph-rms} is the RMS value of the phase voltage, N_{series} is the number of series turns in a phase and K_w is the winding factor.

From the induced EMF equation, for a given E_{ph-rms}, N_{series} is calculated

$$N_{series} = \frac{E_{ph-rms}}{4.44 f \phi_{pp} K_w} \tag{2.31}$$

Since two conductors form a turn and there are three phases, the total number of conductors $z_{q_{total}}$ is given by

$$z_{q_{total}} = 2 * 3 * N_{series} \tag{2.32}$$

Now the number of conductors in a single slot is calculated as:

$$z_q = \frac{z_{q_{total}}}{N_{slots}} \tag{2.33}$$

z_q should always be a whole number because the number of conductors cannot be a fraction or a negative quantity. Also, if the winding is double layered, z_q must always be an even number.
The necessity of having parallel paths in a winding arises due to two cases

- **case 1:** z_q is not an integer. For instance, z_q turns out to be a fraction. In this case, parallel paths are needed to make sure z_q is an integer. To find the number of parallel paths n_{pp}, first fix a value for the number of conductors in a slot - $z_{q_{fix}}$ then

$$n_{pp} = \frac{z_{qfix}}{z_q} \tag{2.34}$$

- **case 2:** The value of E_{ph-rms} is not within a desired range. For example, after design; the value of E_{ph-rms} comes to 1.5 kV when it's maximum value $E_{ph-rms_{limit}}$ is limited to 0.75 kV. In this case,

$$n_{pp} = \frac{E_{ph-rms}}{E_{ph-rms_{limit}}} \tag{2.35}$$

n_{pp} must finally satisfy both the conditions - i.e. deciding n_{pp} for a proper z_q should not lead to E_{ph-rms} going out of range.

Determining slot Area

Assuming all current flows through the q axis, the procedure to determine slot area is [42] [44]:
First the RMS value of phase current (I_{ph-rms}) is calculated from the power generated by the machine (P_{mech}) and E_{ph-rms}

$$I_{ph-rms} = \frac{P_{mech}}{3E_{ph-rms}} \tag{2.36}$$

Next the current through a single conductor (I_{zq}) is determined as:

$$I_{zq} = \frac{I_{ph-rms}}{n_{pp}} \tag{2.37}$$

The current flowing through a single slot I_{slot} is calculated as:

$$I_{slot} = I_{zq}z_q \tag{2.38}$$

For a chosen value of current density (J), the area of copper is calculated as:

$$Ar_{Cu} = \frac{I_{slot}}{J} \tag{2.39}$$

Now for a chosen value of fill factor K_{fill} which is fraction of slot area filled with conductors. The fill factor ranges from 0.4 to 0.6 depending upon the manufacturer. Higher fill factors need rectangular conductors [3]. For this thesis, 0.4 is chosen assuming that the conductors are round. The slot area is calculated as:

$$Ar_{slot} = \frac{Ar_{Cu}}{K_{fill}} \tag{2.40}$$

Finally, slot depth is calculated from area from based on the slot area and slot width.

2.1.5. Calculating Inductance via Analytical method

Calculation of inductance using analytical method is by using winding function theory [29] [22]. The main equations that are used in this analytical model are summarised below [29]

$$L_d = L_{md} + L_0 \tag{2.41}$$

$$L_{md} = \frac{\int_0^{2\pi} \sum_{n=v} \frac{2NK_w}{vp\pi} \cos v\theta_s B_d \frac{(R_s+R_r)}{2} l d\theta_r}{I} \tag{2.42}$$

and

$$L_q = L_{mq} + L_0 \tag{2.43}$$

$$L_{mq} = \frac{\int_0^{2\pi} \sum_{n=v} \frac{2NK_w}{vp\pi} \cos v\theta_s B_q \frac{(R_s+R_r)}{2} l d\theta_r}{I} \tag{2.44}$$

Here L_q is the q axis inductance, L_d is the d axis inductance, L_0 is the leakage inductance
The synthetic armature reaction MMF is determined by

$$F = \frac{3NK_w I}{vp\pi} \tag{2.45}$$

The magnetic potentials at d and q axis are obtained from

$$U_d = \sum_v \frac{2FP1 \sin(\frac{v\alpha\pi}{2})}{v(P_2 + P_3 + P_4 + P_5)} \tag{2.46}$$

and

$$U_q = \sum_v \frac{FP1 \sin(\frac{v(1-\alpha)\pi}{2}) - sin(\frac{v(1-\beta)\pi}{2})}{v(2P_5 + P_6)} \tag{2.47}$$

where Dimensions of the air bubble region and values of α and β are modified from this diagram as
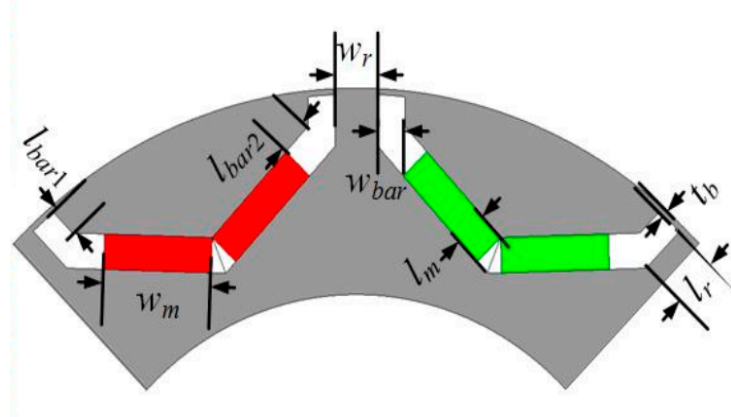
Figure 2.6: Dimensions used [29]

per the geometrical requirements of the thesis geometry.
For the below equations, R_s is the stator bore radius and R_r is the rotor outer radius. P_1 to P_6 are calculated using [29]

$$P_1 = \frac{\mu_0}{p(R_s - R_r)} \frac{R_s + R_r}{2} l \tag{2.48}$$

$$P_2 = P_1 \alpha\pi \tag{2.49}$$

$$P_3 = \frac{2\mu_0\mu_r w_m l}{l_m} \tag{2.50}$$

$$P_4 = \frac{2\mu_0(I_{bar1} + I_{bar2})l}{w_{bar}} \tag{2.51}$$

$$P_5 = \frac{2\mu_0\mu(B_b)t_b l}{w_b} \tag{2.52}$$

$$P_6 = P_1 \frac{(\beta - \alpha)\pi}{2} \tag{2.53}$$

2.2. The Finite Element Method

The Finite Element Method (FEM) is a modelling procedure that is used to solve problems in engineering [14].

2.2.1. Summary of the steps involved in FEM

The steps in FEM modelling are summarised as [14]:

- **Step 1: Geometry:** The geometry of the model is constructed based on fig.1.7.

- **Step 2: Defining Physics:** Various equations (differential equations - Maxwell's equations in case of electrical applications) that govern the model are chosen and the parameters are given. In this thesis, Ampere's Law is used.

- **Step 3: Meshing:** The geometry is divided into small pieces called elements. This is called 'mesh generation'. The mesh can be crude or very fine depending on the accuracy of the final solution finally needed.

- **Step 4: Solving:** The differential equation involved is solved in this step. Flux density is the primary result obtained in case of this thesis.

- **Step 5: Analysis:** The results are of the solution from step 4 are analysed. Further results are derived from the initial results and everything is visualised. In this thesis, flux, flux linkages, induced EMF, torque and inductance are the derived results.

Steps 1 to 4 are done in COMSOL. Step 5 is done in COMSOL and MATLAB via an interface called Livelink.

2.2.2. Equations used in defining physics

Ampere's law from Maxwell's equation is given by [43]:

Ampere's Law - Maxwell's equations:

$$\vec{B} = \nabla X \vec{A} \tag{2.54}$$

For static EM fields

$$\vec{H} = \nabla X \vec{J} \tag{2.55}$$

$$\vec{J} = \sigma \vec{E} \tag{2.56}$$

$\vec{B}$ = Magnetic flux density in T (Tesla)
$\vec{H}$ = Magnetic field intensity in A/m (Ampere per metre)
$\vec{E}$ = Electric field intensity in V/m (Volt per metre) or N/C (Newton per Coulomb)
$\vec{J}$ = current density in A/m^2 (Ampere per square metres)

In order to calculate the induced EMF, the following equations are used [10]

$$E_{ph-rms} = -N_{series}(d\phi/dt) \tag{2.57}$$

$$\phi = \oint_S \vec{B}.\vec{ds} \tag{2.58}$$

To define the physics in COMSOL by selecting surfaces in geometry and thereby calculate the flux linkage of a phase, it is necessary to re-write the equation as shown in eq.2.59

$$\lambda_A = \frac{N_{series}l}{S_{a+}}(\oint_{a+} \vec{A_z}d\vec{S}_a - \oint_{a-} \vec{A_z}d\vec{S}_a) \tag{2.59}$$

Eq.2.57 is rearranged and used to check whether the machine produces required the flux linkages.

$$\lambda_{ph-peak} = \frac{E_{ph-peak}}{w_{elec}} \tag{2.60}$$

2.3. Additional Equations used in Simulation and Analysis

2.3.1. Park and Inverse Park Transforms

The motor used is a three-phase motor. So there are three phases involved - a, b and c. Since all three phases are sinusoidal and balanced with a displacement of 120 degrees; the 3 variable abc reference frame can be converted to a 2 variable dq reference frame. This makes calculations easier. The conversion from abc reference frame to dq reference frame is called Park Transform. Amplitude invariant, a phase to d axis alignment Park transform is used throughout the project [35].

$$\begin{vmatrix} d \\ q \\ 0 \end{vmatrix} = (2/3) * \begin{vmatrix} cos\theta_e & cos(\theta_e - 2\pi/3) & cos(\theta_e + 2\pi/3) \\ -sin\theta_e & -sin(\theta_e - 2\pi/3) & -sin(\theta_e + 2\pi/3) \\ 1/2 & 1/2 & 1/2 \end{vmatrix} \begin{vmatrix} a \\ b \\ c \end{vmatrix}$$

(2.61)

where

$$\theta_e = \omega_e * t + \delta \tag{2.62}$$

in which

$$\omega_e = p * \omega_m \tag{2.63}$$

Inverse Park Transform converts from abc to dq frame [33]

$$\begin{vmatrix} a \\ b \\ c \end{vmatrix} = \begin{vmatrix} cos\theta_e & -sin(\theta) & 1 \\ cos(\theta_e - 2\pi/3) & -sin(\theta_e - 2\pi/3) & 1 \\ cos(\theta_e + 2\pi/3) & -sin(\theta_e + 2\pi/3) & 1 \end{vmatrix} \begin{vmatrix} d \\ q \\ 0 \end{vmatrix}$$

(2.64)

2.3.2. Calculating Torque by Arkkio's Method

Arkkio's method is used to obtain the torque produced by rotating electrical machines during finite element analysis. This method is an improved version of the Maxwell's stress tensor method to find torque. Maxwell's stress tensor is a second rank electromagnetic tensor that represents the interaction between electromagnetic forces and momentum [27].

$$T_{Mstress} = \frac{l}{\mu_0} \int_0^{2\pi} B_r B_\theta r^2 d\theta \tag{2.65}$$

where $T_{Mstress}$ is the torque calculated from Maxwell's stress tensor method, B_r is the radial component

of the flux density in the air-gap, B_θ is the circumferential component of the flux density in the air-gap. This method calculates the total torque on the machine rotor, by integrating the magnetic flux density along any surface completely enclosing the rotor. However, this method has a drawback. If the flux density at the air gap is not correct, it will cause huge errors in the final calculation. This is because the flux density is the curl of vector potential. There is differentiation involved. Error accumulation is very high whenever operations like differentiation are involved.

Arrkio's Torque improves this method by taking integral of several radii that fit inside the air gap and then taking an average. This cancels a large portion of the numerical error.

$$T_{ark} = \frac{l}{\mu_0(r_{out} - r_{in})} \int_0^{2\pi} \int_{r_{in}}^{r_{out}} B_r B_\theta r^2 \, dr \, d\theta \tag{2.66}$$

where T_{ark} is the torque produced as per Arkkio's method, r_{in} to r_{out} is a radius that fits inside the air gap.
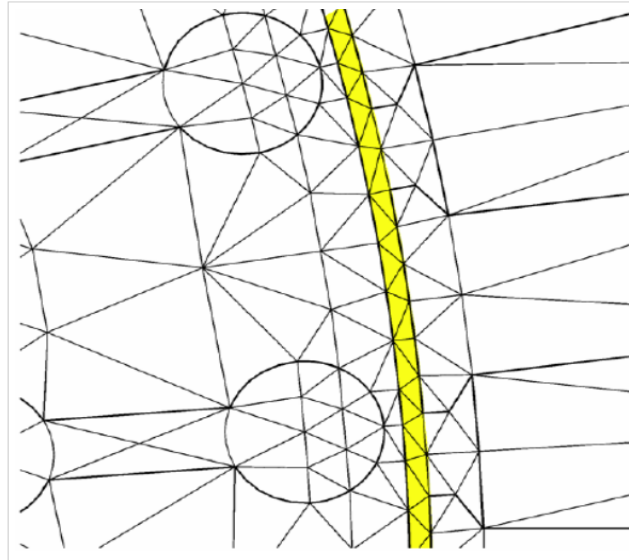
Figure 2.7: Torque computation using Arkkio's method [27].

In this thesis, Arkkio's method is used to validate the torque produced by the machine. In Arrkio's method the geometry and flux density at air gap determine the torque. While in other methods, inductance or flux linkages are used to determine the torque. Since flux linkages depend on the inductance, error caused in calculation of inductance might adversely affect the overall torque calculation. This issue is absent in case of Arkkio's method.

2.3.3. Finding Inductance
In order to calculate the inductance [42]:
First the machine is simulated at no load.
Next the machine is simulated with i_d having a current and i_q being zero.
Then L_d can be calculated

$$L_d = \frac{\lambda_d - \lambda_{d_0}}{i_d} \tag{2.67}$$

Similarly
Next the machine is simulated with i_q having a current and i_d being zero.
Then L_q can be calculated

$$L_q = \frac{\lambda_q - \lambda_{q_0}}{i_q} \tag{2.68}$$

where L_d is the inductance along d axis, L_q is the inductance along q axis, i_d is the current along d axis, i_q is the current along q axis, λ_d is the flux linkage along d axis when i_d is flowing, λ_q is the flux

linkage along d axis when i_q is flowing, λ_{d_0} is the flux linkage along d axis and λ_{q_0} is the flux linkage along q axis when both i_d and i_q are zero (No load condition).

2.3.4. Finding the optimal current to simulate

If directly Lagrange's Multiplier's is used then; the function to optimise is

$$F(x,y) = \sqrt{(i_d^2 + i_q^2)} \tag{2.69}$$

Here the objective is to find the minimum value of current to produce the desired torque. The program automatically chooses the minimum value and hence there is no need give any special symbol to minimise. However if the objective is to maximise the given function, a negative symbol has to be given in F(x,y)
The constraint function

$$g(x,y) = \frac{3}{2}p[\psi_m i_q + (L_d - L_q)i_d i_q] - T_{em} \tag{2.70}$$

Optimal current using Maximum Turn Per Ampere Method (MTPA)

Maximum Turn Per Ampere Method (MTPA) is an imaginary axis of the current locus diagram. Choosing an operating trajectory along this line will lead to the selection of a of an operating point with the lowest oh-mic losses [9].
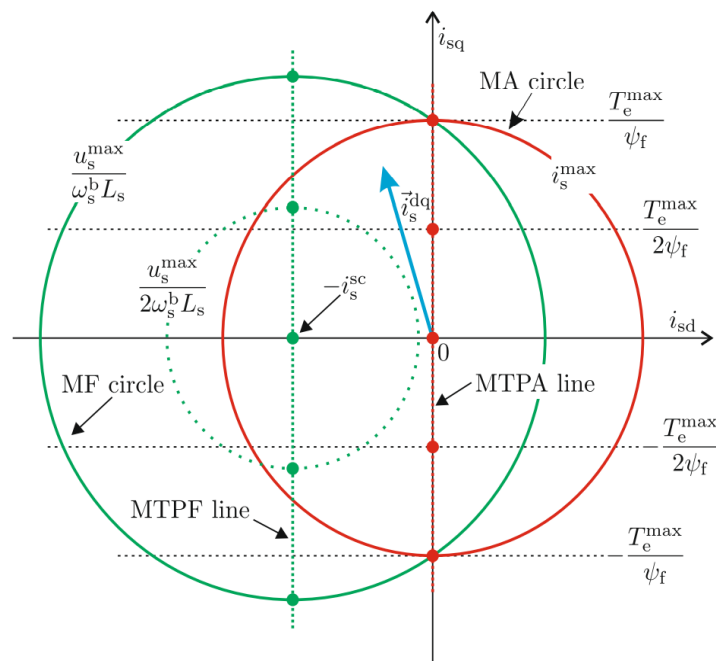
Figure 2.8: Operational drive limits for non-salient synchronous drives.[9]

The value of i_d can be obtained from the below equations used in MTPA control strategy [17]:

$$i_d = \frac{-\psi_m + \sqrt{\psi_m^2 + 4(L_d - L_q)^2 i_q^2}}{2(Ld - Lq)} \tag{2.71}$$

Where ψ_m is the magnet flux
Now i_q can be determined from

$$i_q = \sqrt{i_s^2 - i_d^2} \tag{2.72}$$

where i_s is the stator current.

Using MTPA method directly gives the maximum torque for a fixed stator current. In order to obtain the minimum current for a fixed torque, the MTPA equations are modified and used as given in equations from eq. 2.73 to eq. 2.84 [51]:

$$T_{em} = 1.5p\psi_m i_q + 1.5p(L_d - L_q)i_d i_q \tag{2.73}$$

$$T_{ex} = 1.5p\psi_m i_q \tag{2.74}$$

$$T_{rel} = 1.5p(L_d - L_q)i_d i_q \tag{2.75}$$

T_{em} is the electromagnetic torque, T_{ex} is the excitation torque, T_{rel} is the reluctance torque.

$$I_b = \frac{\psi_m}{2(L_d - L_q)} \tag{2.76}$$

$$T_b = 0.75p\psi_m I_b \tag{2.77}$$

I_b is the base current and T_b is the base torque.

For the rest of the equations to find the optimal current, a per unit model is used. $T_{emu} = (\frac{T_{em}}{T_b})$ is the per unit value of T_{em}, $T_{relu} = (\frac{T_{rel}}{T_b})$ is the per unit value of T_{rel}, $T_{exu} = (\frac{T_{ex}}{T_b})$ is the per unit value of T_{ex}, $i_{su} = (\frac{i_s}{I_b})$ is the per unit value of i_s, $i_{du} = (\frac{i_d}{I_b})$ is the per unit value of i_d, $i_{qu} = (\frac{i_q}{I_b})$ is the per unit value of i_q,

Using, the per unit parameters, the per unit model is developed. The equations of torque in per unit quantities are:

$$T_{emu} = 2i_{qu} - i_{qu}i_{du} \tag{2.78}$$

$$T_{relu} = -i_{qu}i_{du} \tag{2.79}$$

$$T_{exu} = 2i_{qu} \tag{2.80}$$

The equations of stator current in per unit quantity is:

$$i_{su}^2 = i_{du}^2 + i_{qu}^2 \tag{2.81}$$

Using equations 2.78 to 2.80 in 2.83, the expression for current in terms of torque becomes:

$$i_{qu} = \frac{T_{emu}}{2 - i_{du}} \tag{2.82}$$

Using eq. 2.82 in eq. 2.83:

$$i_{su}^2 = i_{du}^2 + \frac{T_{emu}^2}{(2 - i_{du})^2} \tag{2.83}$$

Differentiating eq.2.83 with respect to i_{du} and equating it to zero, the minimum value of i_{su} is obtained:

$$\frac{di_{su}^2}{di_{du}} = 2i_{du} + \frac{2T_{emu}^2}{(2 - i_{du})^3} = 0 \tag{2.84}$$

Eq.2.84 gives the minimum value of current for a given fixed torque. But since the equation is quartic, it becomes difficult to solve it [51]. Hence finding a minimum value of current for a given torque using the MTPA concept becomes a hard task.

2.4. Optimisation

Multi-objective optimisation is needed when there is more than one objective to optimise with a conflict between the objectives. In this thesis, there are three objectives to optimise - increase total efficiency, reduce total volume and reduce the magnet weight.

2.4.1. Optimisation Techniques used in general

There are several optimisation techniques and it is difficult to decide which one to select - especially in case of multi objective optimisation. Two of the most commonly used multi objective optimisation techniques are Multi Objective Genetic Algorithm and Multi Objective Particle Swarm. Since real life problems come in with many limits and constraints, the suitability of algorithm depends entirely upon the application [49].

Genetic Algorithm (GA)

GAs are based on the theory of natural selection and evolution which in turn depends upon the survival of the fittest. Over time, population adapts to the environment and the most suitable population would survive while the rest fail [49].
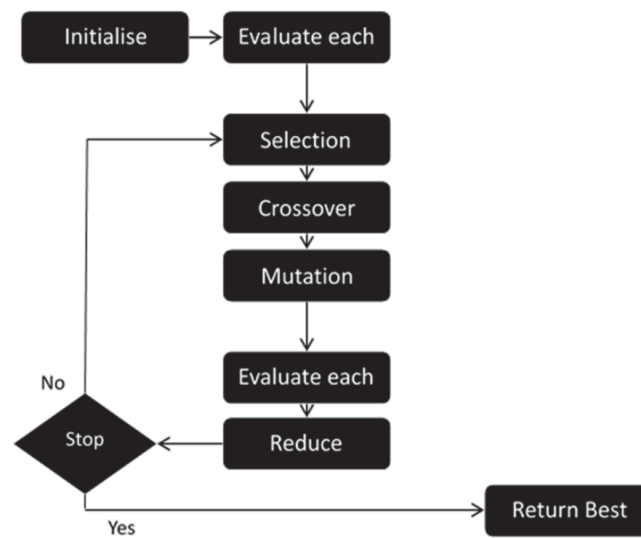
Figure 2.9: Flow Chart of Genetic Algorithm. [49]

Particle Swarm Optimisation (PSO)

PSO is a population based algorithm that was inspired from the social behaviour of flocks of birds. In PSO, each solution is called a particle and the whole population is called the swarm. PSO is popular in optimizing problems with real numbers [49].

In order to decide which algorithm to select among GA and PSO - first the advantages and disadvantages of both the algorithms are studied. Next the suitability of these algorithms particularly in the case of optimisation of machines is considered carefully. And finally the ease of implementing this in MATLAB is taken into consideration.

2.4.2. Comparison of PSO and GA

The below advantages and disadvantages are taken from a study on a review of optimization techniques applied for the integration of distributed generation from renewable energy sources [4].

From the table 2.1, it can be observed that both GA and PSO have several advantages as well as disadvantages. A disadvantage that is common to both is the tendency to get trapped in a local optima. Speed appears to be the single largest advantage PSO has over GA. While the main advantage GA has over PSO is its ability to arrive at a sufficiently accurate end result even if other in between solutions are bad.

Apart from the comparison in table 2.1, from a general qualitative comparison of algorithms, it was found
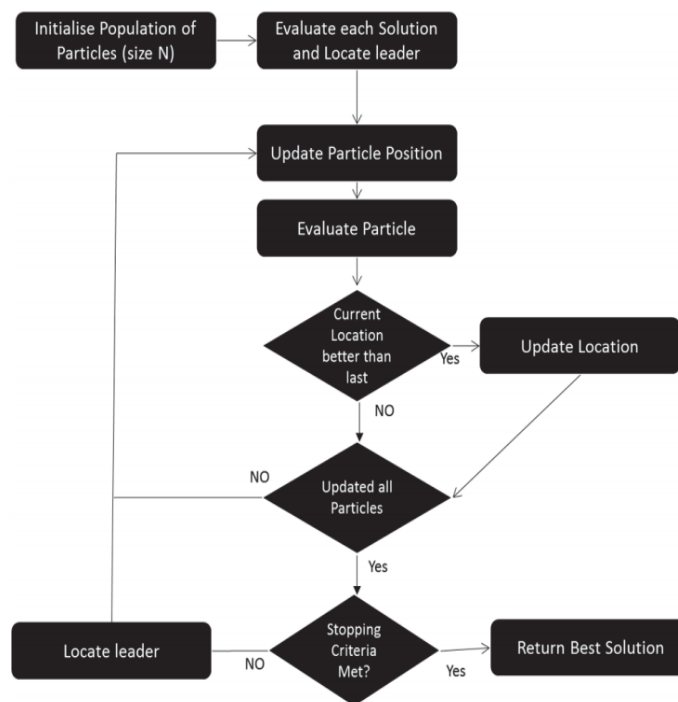
Figure 2.10: Flow Chart of Particle Swarm Optimisation. [49]

Features	Genetic Algorithm (GA)	Particle Swarm Optimisation (PSO)
Advantages	Derivatives are not required	Can be easy to implement
	For a wide variety of functions, there is a better chance of finding a global optimal solution.	Higher probability and efficiency in finding a global optimal solution
	Can be applied using both continuous and discrete parameters.	Have fewer parameters to adjust
	Possible to apply this to problems that are complex and are not well defined	Has the ability to run parallel computations and is efficient for solving problems where it is difficult to find accurate mathematical models.
	The final result is not adversely affected by poor solutions	Can be robust. It doesn't easily overlap and mutate
		Has fast convergence
Disadvantages	Since repeated fitness function evaluation occurs, it can turn out to be time consuming if the problem involved is large and complex	Can be difficult to define initial parameters
	Can be trapped in local optima	Can be trapped in local optimum due to premature convergence when complex problems are involved
	Can be inaccurate and suggest bad solutions	Is not able to work out the problem of scattering

Table 2.1: Comparison of PSO and GA [4].

that the population size has a linear influence on time for PSO and an exponential influence on time in csae of GA. But PSO has higher rates of premature convergence compared to GA [23]. Now looking at literature that compares PSO and GA specifically for the purpose of optimisation of permanent magnet machines, it is seen that PSO should be preferred over GA whenever time is a limiting factor [11].
When it comes to implementation of multi-objective algorithms in MATLAB, a standard code for multi-objective GA is already developed and widely in use in the optimisation toolbox whereas one has not yet been developed for multi-objective PSO though may researchers have proposed widely accepted algorithms [34] [54].

Since the initial model of the machine was designed and not already available, the probability of the first set of design parameters being close to the actual solution is uncertain. As it is hard to define initial parameters in PSO and considering the fact that that GA has a better capability of delivering end solution correctly; GA is more suitable in this regard.
PSO has the ability to compute in a parallel manner which makes it inherently suitable for multi - objective algorithms. But another factor is that because already established multi-objective algorithms are available in existing toolbox, implementing multi objective GA will not be a problem.
The third factor is the rate of convergence where PSO is faster than GA. For this thesis, analytical model is used for optimisation and not the FEM model. Hence time is not going to be an issue.
Considering all these three points, GA is more suitable for this particular thesis.

2.4.3. Key Concepts in Genetic Algorithm

Genetic Algorithm (GA) is a search algorithm that is based on the evolutionary ideas of natural genetics [31].
Many conventional optimisation algorithms start with one candidate and repetitively searches for an optimal solution by heuristic search. In contrast to this, GA uses a population of candidates to search several areas of a solution space at the same time in an adaptive manner [48]. Basically what GA does is that it generates a population of high quality primary individuals where each individual represents a solution for the problem [31]. Usually, GA have been employed to solve combinatorial optimization problems that have a large number of solutions [48].

Summary of GA Implementation [48]

- First an initial population set is randomly generated. The initial population size should be sufficiently high. Typical population sizes vary between 30 and 200. Population diversity should also be sufficiently high for the solution to converge. Hence care should be taken while applying prior knowledge about the solution to the initial population so that population diversity is not compromised.

- Then, GA is executed in two steps. Step 1: Starting with the present initial population, selection is applied to create an intermediate population (mating pool).

- Step 2: Crossover and mutation are applied to the present intermediate population to create the next generation of potential solutions.

Though manual tuning of parameters is common in GA, this is at the risk of obtaining sub optimal solutions. In case of manual tuning, one parameter is dealt with at a time instead of simultaneous estimation to avoid difficult challenges [48].
Using GA as such, it is difficult to get a solution. One of the key aspects in using GA is the need to tailor basic operators.
Basic operators in GA: There are three basic operators in GA - selection, mutation and crossover. They are explained as [48]:
Selection
Selection is the operator that determines the characteristics of convergence in GA. Selection pressure is the degree to which the best individuals are favoured and is directly proportional to the number of best individuals being favoured. The selection intensity of GA is the expected change of average fitness in a population after selection is performed. Analyses of selection schemes show that the change in mean fitness at each generation is a function of the population fitness variance. The selection pressure determines the rate of convergence. For faster convergence, higher selection pressure is needed. If the

selection pressure is too low, GA takes a longer period to search for the solution implying that the rate of convergence would be very slow. However if the selection pressure is too high, then convergence rate would be too fast. This would prematurely lead to a rapid convergence rate to a bad solution Apart from selection pressure, selection should also ensure that population diversity is preserved. One possible way to achieve this goal is to maximize the product of selection intensity and population fitness standard deviation. Therefore, if two selection methods have the same selection intensity, the method giving the higher standard deviation of the selected parents is the best choice [48].

Mutation

The primary function of mutation is to maintain diversity within population and to prevent premature convergence to local optimal point. This is accomplished by randomly sampling new points in the search space. So basically what mutation does is that it explores new areas in the search space. Hence, mutation determines the search efficiency and is more critical than crossover rate. The importance of the mutation operator is at the time of final generations when there a large number of similar individuals in the population. Typical mutation rate is [0.001; 0.05] [48].

Constant parameters in GA will lead to an inferior performance because GA is adaptive in nature. In case of implementation of mutations; during early generation - there must be large number of mutations. This is to increase exploration. However towards the end, the number of mutations must be kept low so as to get finer solutions [48].

Crossover

Crossover is the recombination (mating) of two individuals. Two new individuals are formed when parts of strings of the original two individuals are exchanged. The easiest way crossover happens is when after randomly choosing a crossover point, the interchange of sub-strings take place. Range of crossover operator is [0.5, 1.0]. What crossover does is that it enables evolutionary process to move towards better and more favourable regions of the search space. In order to create better offspring, portions of good individuals must be recombined [48].

Since information is split during crossover, it is considered to be a disruptive operator and is controversial in nature. How useful crossover turns out to be is dependent upon the problem. The traditional GA uses one-point crossover where the two parents are each cut once at specific points and the segments located after the cuts exchanged as illustrated in the fig. 2.11 [48].

$$[1 \ 1 \ | \ 0 \ 1 \ 0 \ 1 \ 0 \ 1] \ [1 \ 1 \ 0 \ 1 \ 1 \ 0 \ 0 \ 0]$$

$$\Rightarrow$$

$$[1 \ 0 \ | \ 0 \ 1 \ 1 \ 0 \ 0 \ 0] \ [1 \ 0 \ 0 \ 1 \ 0 \ 1 \ 0 \ 1]$$

Example of one-point crossover.

Figure 2.11: Illustration of one crossover point [48]

After crossover operation takes place, the probability of the bits remaining together is decided by the position of the bits in the schema. Since one of the offspring always inherits the critical bit, recombination does not influence an order-1 schema. The crossover operator for a single crossover point can be generalized in order to apply multiple-point crossover. The higher the crossover points, the better the exploration capacity with a serious disadvantage of causing too much disruption. Due to this reason, more than two crossover points are not used [48].

2.4.4. Multi-objective GA

Multi objective GA is GA with multiple objectives. The flow chart of multi-objective GA is same as GA with the inclusion of additional objectives.

2.4.5. Formulation of multi-objective functions

Objective 1: Minimise Losses

The first objective is to minimise the losses involved. By minimising losses, the efficiency is maximised.
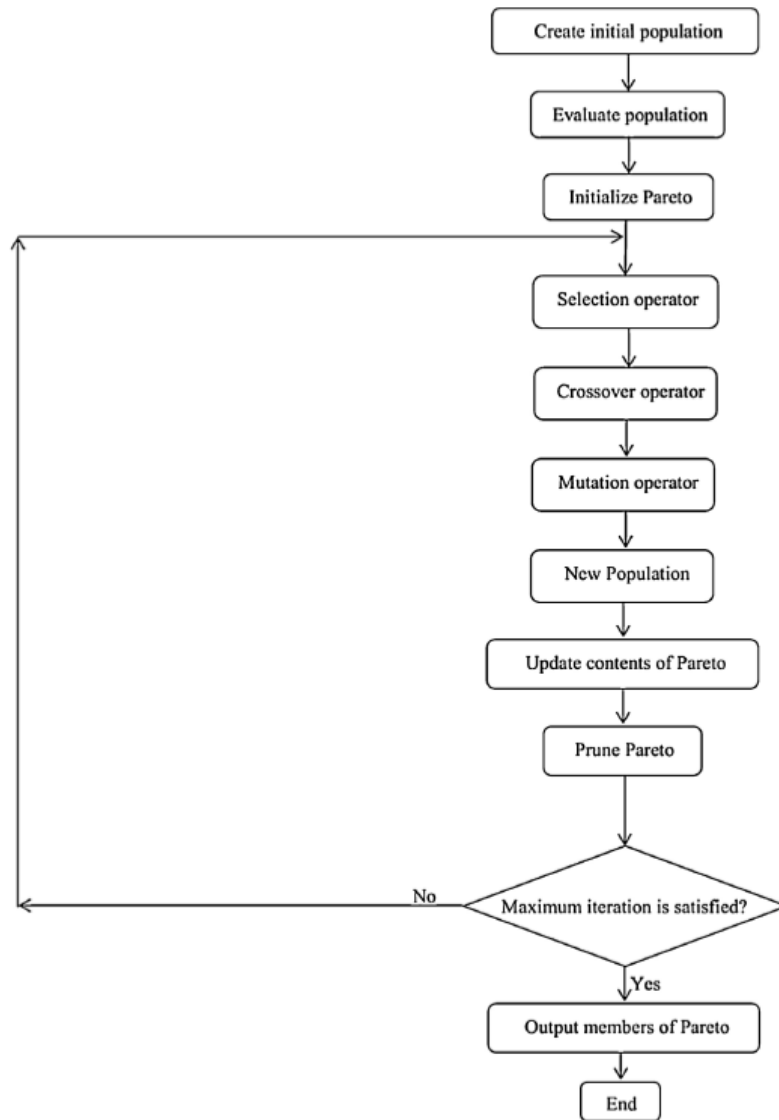
Figure 2.12: Flow chart of multi-objective GA [31].

The main losses present in a machine are copper loss, iron loss, additional loss and mechanical loss [42]. In the optimisation algorithm developed here, both copper loss and iron loss are considered.

Copper Loss

Copper loss is calculated as [42]:

$$P_{cu} = 3I_{ph-rms}^2 R_{AC} \tag{2.85}$$

R_{AC} is the AC resistance of the phase winding by eq.2.86.

$$R_{AC} = k_R \frac{N l_{av}}{\sigma S_c} \tag{2.86}$$

Where k_R is the skin effect factor, N is the number of turns, l_{av} is the average length of a turn, S_c is the cross-sectional area of the conductor and σ is the specific conductivity of the conductor
If there are n_{pp} parallel paths, then the above equation becomes

$$R_{AC} = k_R \frac{N_{series} l_{av}}{\sigma S_c n_{pp}} \tag{2.87}$$

where N_{series} is the number of series turns per phase

$$l_{av} = 2l + 2.4W + 0.1m \tag{2.88}$$

where l = axial length in metres and W is the coil span in metres

In this case, the skin effect factor k_R is considered as 1. This is because the skin effect factor depends upon the manner in which the conductors are connected inside the slot and the shape of the conductors. If they are transposed, then the skin effect is negligible [42]. In the model here, only the current density and number of conductors per slot are involved and hence it is sufficient to consider the skin effect factor to be 1.

Iron Loss

Iron losses are classified as hysteresis loss and eddy current loss. Hysteresis is the phenomenon where throughout the magnetisation cycle, the magnetic flux density lags behind the magnetic intensity [47]. Hysteresis loss is the loss caused due to the material in an alternating field [42]. Hysteresis loss is illustrated in fig. 2.13.
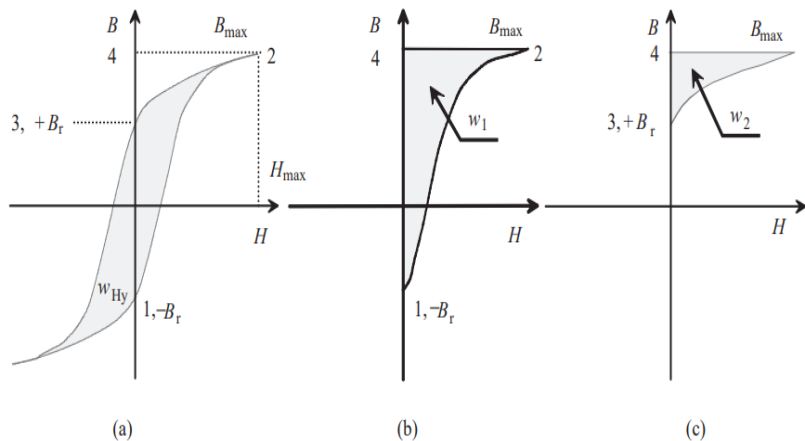
Determination of hysteresis loss: (a) entire hysteresis curve, (b) w_1, magnetic energy per volume stored when moving from 1 to 2, (c) w_2, magnetic energy per volume returned when moving from 2 to 3

Figure 2.13: Hysteresis loss [42]

Eddy current losses occur due to eddy currents which are a consequence of alternation of flux and corresponding induced voltages in the conductive core material. Laminations or high-resistivity compounds are used to restrict the effect of eddy currents [42].
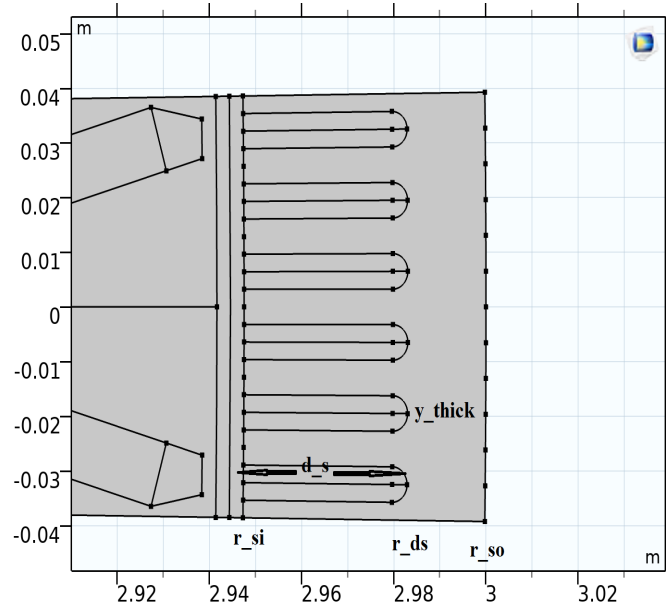
Figure 2.14: Picture showing parameters used to calculate volume of both teeth and yoke

$$Ar_{all-slots} = Ar_{slot}N_{slots} \tag{2.89}$$

$$V_{Si} = [\pi(r_{so}^2 - r_{si}^2) - Ar_{all-slots}]l \tag{2.90}$$

$$y_{thick} = (r_{so} - r_{si}) - d_s \tag{2.91}$$

Where d_s is the slot depth.

$$r_{ds} = r_{so} - y_{thick} \tag{2.92}$$

$$Ar_{teeth-plus-slots} = \pi(r_{ds}^2 - r_{si}^2) \tag{2.93}$$

$$Ar_{teeth} = \pi(r_{ds}^2 - r_{si}^2) - Ar_{all-slots} \tag{2.94}$$

$$V_{teeth} = [\pi(r_{ds}^2 - r_{si}^2) - Ar_{all-slots}]l \tag{2.95}$$

$$V_{yoke} = V_{Si} - V_{teeth} \tag{2.96}$$

Finding Magnetic Flux Density at Teeth and Yoke
Magnetic Flux Density at Teeth

$$B_{teeth} = \frac{B_g(w_t + w_s)}{w_t} \tag{2.97}$$

Magnetic Flux Density at Yoke

$$A_{yoke} = y_{thick}l \tag{2.98}$$

$$B_{yoke} = \frac{\frac{\Phi_{pp}}{2}}{A_{yoke}} \qquad (2.99)$$

Step III - Calculating Loss

$$P_{Fe} = \sum_n k_{Fe,n} P_{15} \left(\frac{\hat{B}_n}{1.5T}\right)^2 m_{Fe,n} \qquad (2.100)$$

Where P_{15}=4W/kg,1.5T,50Hz Since the above formula calculates the iron loss per element and sums it all up, hysteresis loss has to be calculated for both yoke and teeth separately
Iron Loss in Yoke

$$P_{Fe_{yoke}} = k_{Fe_y} P_{15} \left(\frac{\hat{B_{yoke}}}{1.5T}\right)^2 m_{yoke} \qquad (2.101)$$

where k_{Fe_y} is the correction coefficient of iron loss at yoke taken as 1.5 [42]
Mass of the yoke is calculated as below where

$$m_{yoke} = \rho_{Si_{steel}} * V_{yoke} \qquad (2.102)$$

Iron Loss in Teeth

$$P_{Fe_{teeth}} = k_{Fe_t} P_{15} \left(\frac{\hat{B_{teeth}}}{1.5T}\right)^2 m_{teeth} \qquad (2.103)$$

where k_{Fe_t} is the correction coefficient of iron loss at teeth taken as 2, [42]
Mass of the teeth is calculated as below where

$$m_{teeth} = \rho_{Si_{steel}} * V_{teeth} \qquad (2.104)$$

The total iron loss now is

$$P_{iron} = P_{Fe_{teeth}} + P_{Fe_{yoke}} \qquad (2.105)$$

The total loss which is a combination of both copper and iron loss that is minimised in the algorithm

$$P_{loss} = P_{cu} + P_{Fe_{iron}} \qquad (2.106)$$

Objective 2: Minimise volume
The second objective is to minimise total volume Where the total Volume of the machine is given by

$$V_{total} = \pi r_{so}^2 l \qquad (2.107)$$

Objective 3: Minimise Magnet Weight
For a single rectangular portion,

$$W_{piece} = \rho_{mag} l_m h_m l \qquad (2.108)$$

Since one pole consists of 2 such pieces and the machine has 240 such poles,

$$W_{total-magnets} = 480 * W_{piece} \qquad (2.109)$$

2.4.6. Pareto Solution
When there are multiple objectives in an optimisation problem, the final solution is not a single solution but a set of solutions. This set of solutions is called Pareto-optimal solutions [36].
In a Pareto set of solutions, no solution is better than another. Thus choosing one solution is at the compromise of another objective's best solution.
This makes choosing a single set of solution hard. Hence in this case, the objectives must be weighted so that a solution can finally be selected from the Pareto set.
The main disadvantage of this approach is that the final solution selected depends on the weightage given to individual objectives
 In the example case illustrated in fig.2.15 , the Pareto set is a range of solutions starting from -2 and ending at 2. There is no overall best solution and any solution from the set will be at the compromise of one of the objective's. If the weightage is equal for both the objectives, then the solution in the middle has to be chosen. Else a solution towards the weighted priority has to be selected.
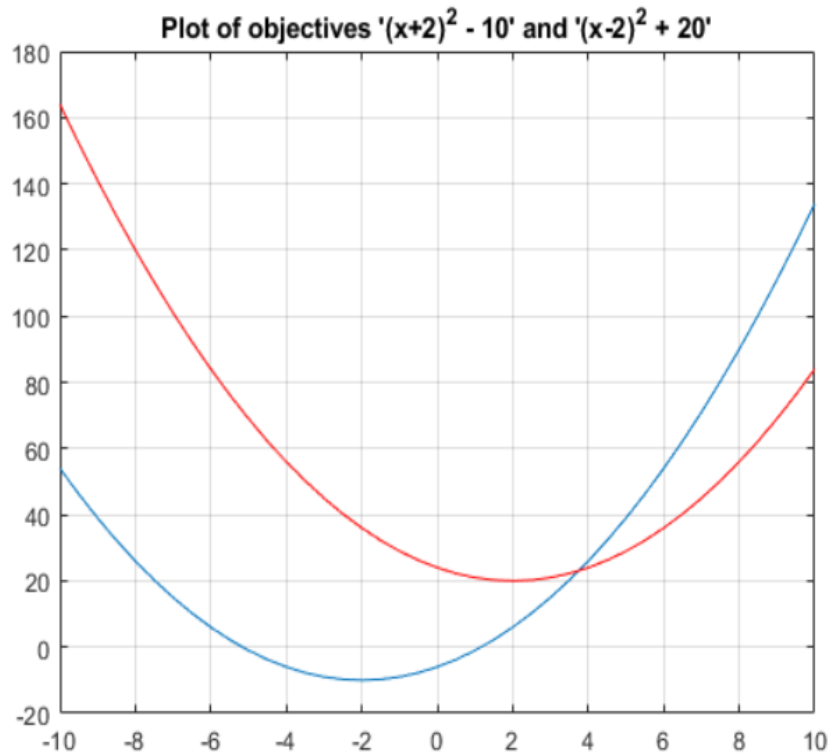
Figure 2.15: Illustration of Pareto Solution [36].

2.4.7. Summary

In this chapter, the design methodology is discussed in detailed. First the analytical model is described which consists of the sizing of machine, the magnetic circuit of rotor, the stator design that includes design of winding plus calculation of slot area and the analytical method of finding inductance. This is followed by the description of the steps involved in FEM modelling. Specifically, important selections in physics are explained. The next section consists of additional equations that are needed for simulation and analysis where equations for Park and inverse Park transform, torque calculation using Arkkio's, FEM calculation of inductance and the method to find the optimal current are written. The next section consists of the theory behind optimisation, selection of GA over PSO, operators and flow chart of GA, formulation of multi-objective functions and the pareto solutions are explained in detail.

<div style="text-align: right; font-size: 3em;">3</div>

Design of the Initial Model

3.1. Analytical Modelling of the Machine

Throughout the thesis, the below parameters are fixed as given in the objective:

Parameters	Value
Output Power	1 MW
Radius of blade tip	12 m
Speed	10 RPM

Table 3.1: Permanently Fixed Parameters

Additionally for the ease of design, the frequency and the number of slots are kept fixed for the chosen topology.

Parameter	Value
Frequency (f)	20 Hz
Number of slots (N_{slots})	1440

Table 3.2: Additional parameters that remain fixed

The number of slots was decided based on the stator design discussed in section 2.1.3 as well as the selected topology on fig.1.7 which is for a 48 slot 8 pole machine [13]. The value of 20 Hz as the frequency was chosen as a starting point considering that frequency was not a fixed parameter and that frequency converters could be used. Now that the frequency is fixed, the number of poles are obtained which is 240. On comparison with the selected topology as well as checking the divisibility by 6, the number of slots is obtained as 1440.

3.1.1. Determining basic parameters

Since only very few parameters are fixed and there is a greater flexibility regarding the range of parameters; some of parameters shown in table 3.3 are kept fixed for the initial design. Later these parameters are varied during optimisation in order to obtain a better value.

Radius of outermost blade tip is fixed at 12m. Radius of the machine should not exceed around one forth of this value. This is because a large machine would lead to a considerable amount of volume not being used in generation of power.

Considering the design of magnets; higher α means more space usage by the magnets. However very high values of α may result in the inability to fix magnets inside the allotted region.

From the permissible value of B_g from fig.3.1, a value of 0.9T is selected as the air gap flux density for this machine.

Parameter	Description	Value Assumed
r_{so}	Stator outer radius	3
k_{si}	Ratio of stator inner radius to stator outer radius	0.9825
k_{wt}	Ratio of slot teeth to slot pitch	0.5
α	Pole arc to pole pitch ratio	0.8

Table 3.3: Assumed values of some basic parameters

Permitted flux densities of the magnetic circuit for various standard electrical machines

	Flux density B/T			
	Asynchronous machines	Salient-pole synchronous machines	Nonsalient-pole synchronous machines	DC machines
Air gap	0.7–0.90 ($\hat{B}_{\delta 1}$)	0.85–1.05 ($\hat{B}_{\delta 1}$)	0.8–1.05 ($\hat{B}_{\delta 1}$)	0.6–1.1 (B_{max})
Stator yoke	1.4–1.7 (2)	1.0–1.5	1.1–1.5	1.1–1.5
Tooth	1.4–2.1 (stator)	1.6–2.0	1.5–2.0	1.6–2.0
(apparent maximum value)	1.5–2.2 (rotor)			(compensating winding) 1.8–2.2 (armature winding)
Rotor yoke	1–1.6 (1.9)	1.0–1.5	1.3–1.6	1.0–1.5
Pole core	—	1.3–1.8	1.1–1.7	1.2–1.7
Commutating poles	—	—	—	1.3

Figure 3.1: Permissible values of B_g [42]

Permitted RMS values for current densities J and linear current densities A for various electrical machines. Depending on the size of a permanent magnet machine, a synchronous machine, an asynchronous machine or a DC machine, suitably selected values can be used. Copper windings are generally assumed

		Sailent-pole synchronous machines or PMSMs	Nonsalient-pole synchronous machines			
			Indirect cooling		Direct water cooling	
	Asynchronous machines		Air	Hydrogen		DC machines
A/kA/m	30–65	35–65	30–80	90–110	150–200	25–65
	Stator winding	Armature winding		Armature winding		Armature winding
J/A/mm^2	3–8	4–6.5	3–5	4–6	7–10	4–9
	Copper rotor winding	Field winding:				Pole winding
J/A/mm^2	3–8	2–3.5				2–5.5
	Aluminium rotor winding	Multi-layer		Field winding		Compensating winding
J/A/mm^2	3–6.5	2–4	3–5	3–5	6–12	3–4
		Single-layer	With direct water cooling, in field windings 13–18 A/mm^2 and 250–300 kA/m can be reached			

Figure 3.2: Permissible values of J [42]

From the permissible value of J from fig.3.2, a value of $6.5 * (10^6)$ A/m^2 is selected as the current density for this machine.

3.1.2. Rotor Design: Solution of the Magnetic Circuit

The Magnetic Circuit is solved using the equations in chapter 2 section 2.1.2. For this rotor, the width of the magnet h_m is calculated to be 0.012148m and the length of the magnet l_m is calculated to be 0.091113m.

3.1.3. Stator Design: Winding Design

The winding pattern is calculated using the winding calculator tool [2]. The winding pattern with the lowest 5th and 7th harmonic is selected for implementation.

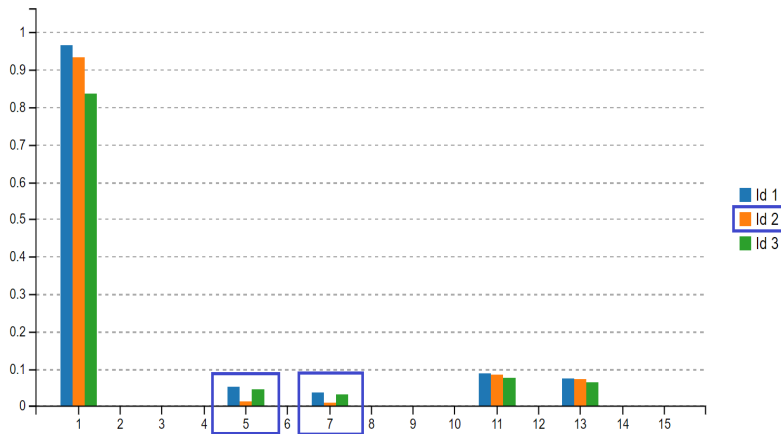| Poles	Slots	Layers	Coil span	Pole pitch	Periodicities	Winding factor
2	12	1	6 slots	6 slots	2	0.966
2	12	2	5 slots	6 slots	2	0.933
2	12	2	4 slots	6 slots	2	0.837

Figure 3.3: Possible Winding Layouts [2]

Figure 3.4: Corresponding Harmonics [2]

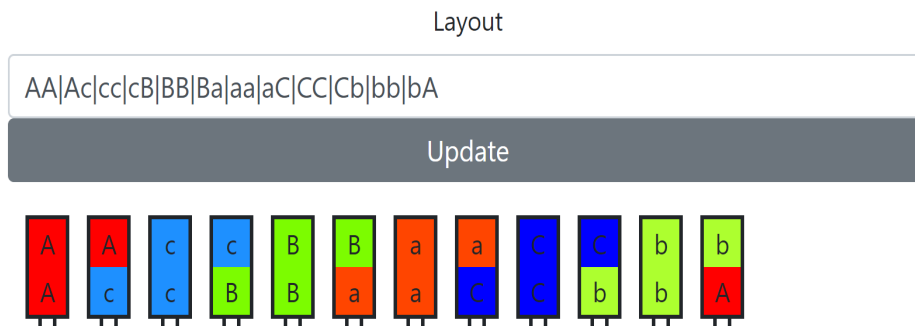Since the second winding layout has the least 5th and 7th harmonics, it was chosen as the winding layout for this model.

Figure 3.5: Current Sequence for the selected layout [2]

Term	Description
Basic features	Double layer, short pitch, distributed
Slots per pole	1440 slots, 240 poles reduced to 12 slots 2 poles
Coil Span	5 slots

Table 3.4: Basic features of stator

3.1.4. Stator Design : Number of parallel paths and area of slot

Based on the design methodology discussed in the section 2.1.4, the number of parallel paths is determined as shown in fig.3.6.
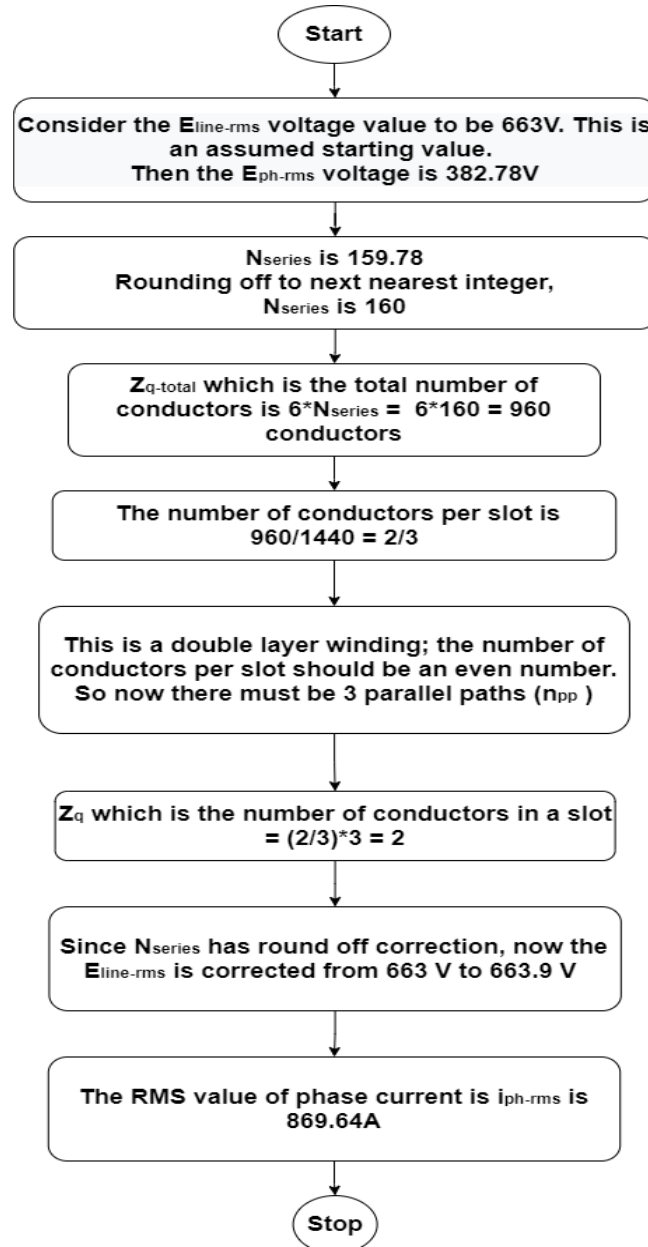
```
                          ╭──────────╮
                          │  Start   │
                          ╰──────────╯
                               │
                               ▼
    ┌─────────────────────────────────────────────────────┐
    │ Consider the E_line-rms voltage value to be 663V.    │
    │ This is an assumed starting value.                   │
    │ Then the E_ph-rms voltage is 382.78V                 │
    └─────────────────────────────────────────────────────┘
                               │
                               ▼
    ┌─────────────────────────────────────────────────────┐
    │ N_series is 159.78                                   │
    │ Rounding off to next nearest integer,                │
    │ N_series is 160                                      │
    └─────────────────────────────────────────────────────┘
                               │
                               ▼
    ┌─────────────────────────────────────────────────────┐
    │ Z_q-total which is the total number of               │
    │ conductors is 6*N_series = 6*160 = 960               │
    │ conductors                                           │
    └─────────────────────────────────────────────────────┘
                               │
                               ▼
    ┌─────────────────────────────────────────────────────┐
    │ The number of conductors per slot is                 │
    │ 960/1440 = 2/3                                        │
    └─────────────────────────────────────────────────────┘
                               │
                               ▼
    ┌─────────────────────────────────────────────────────┐
    │ This is a double layer winding; the number of        │
    │ conductors per slot should be an even number.        │
    │ So now there must be 3 parallel paths (n_pp )        │
    └─────────────────────────────────────────────────────┘
                               │
                               ▼
    ┌─────────────────────────────────────────────────────┐
    │ Z_q which is the number of conductors in a slot      │
    │ = (2/3)*3 = 2                                        │
    └─────────────────────────────────────────────────────┘
                               │
                               ▼
    ┌─────────────────────────────────────────────────────┐
    │ Since N_series has round off correction, now the     │
    │ E_line-rms is corrected from 663 V to 663.9 V        │
    └─────────────────────────────────────────────────────┘
                               │
                               ▼
    ┌─────────────────────────────────────────────────────┐
    │ The RMS value of phase current is i_ph-rms is        │
    │ 869.64A                                              │
    └─────────────────────────────────────────────────────┘
                               │
                               ▼
                          ╭──────────╮
                          │  Stop    │
                          ╰──────────╯
```

Figure 3.6: Calculation of number of parallel paths

Slot area is calculated as shown in fig.3.7 based on the design methodology in section 2.1.4.

Parameter	Value
$E_{line-rms}$	663.9 V
E_{ph-rms}	383.3 V
i_{ph-rms}	869.64 A
N_{total}	480
N_{series}	160
Z_q	2
n_{pp}	3

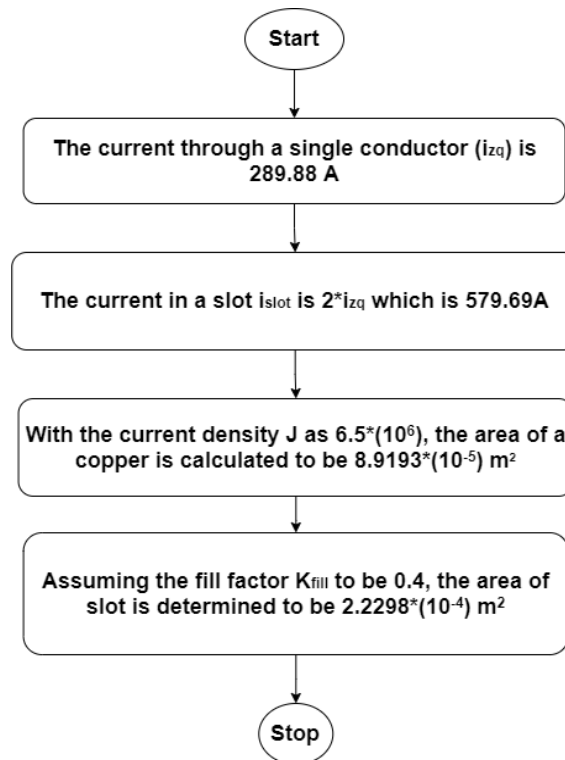Table 3.5: Machine details after stator design

Figure 3.7: Calculation of stator slot area

3.2. FEM Model of the Machine

3.2.1. Step 1: Geometry

The geometry used for FEM (fig.3.8) is initially constructed based on the topology in fig.1.7 such that many of the parameters like k_{si}, k, k_{wt}, α remain as variables and these parameters are used as design variables during optimisation. Geometrical construction involves drawing arcs and lines based on precise coordinate calculation with Boolean logic used to combine them. Rotor and stator are constructed separately and are assembled at the air gap region.

The materials used are listed in 3.6

Geometry	Material
Magnets	Non Linear Permanent Magnet
Stator core	Silicon Steel NGO 35JN200
Rotor core	Low Carbon Steel Pure, Annealed

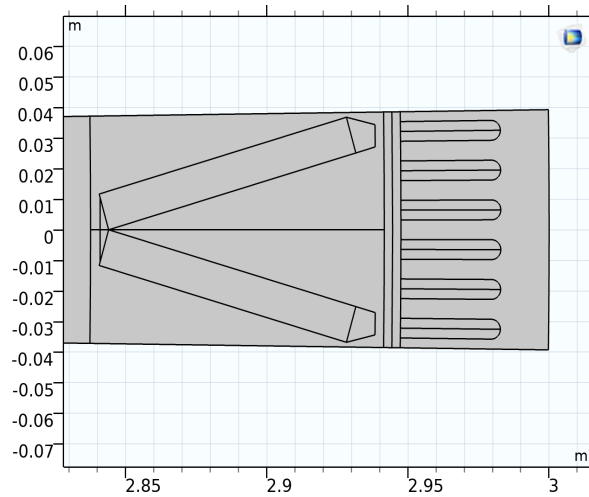Table 3.6: Material Selection

Figure 3.8: Geometry of the Initial Model

3.2.2. Step 2: Defining Physics of the Model

Physics of the magnet is defined by finding the correct vector, choosing the equations and then finally by setting appropriate boundary conditions.
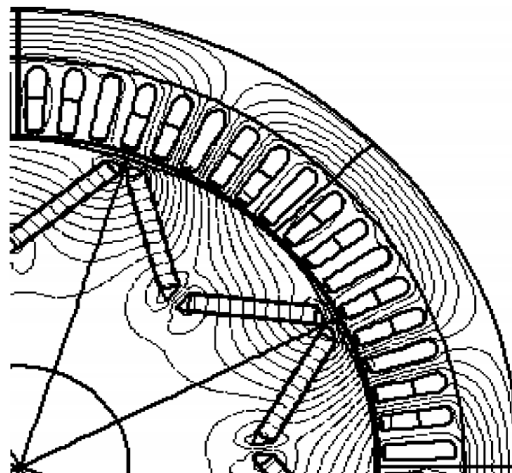

Figure 3.9: Concentration of flux in the V-pole design [25]

The 'V' type magnet produces a flux density as shown in fig.3.9 [25]. In this case, one 'V' set of magnets comprises of a single pole. The physics in COMSOL is defined such that the correct flux density is produced.

After defining the vector as shown in fig.3.10, the magnets are modelled using the remanent flux density equation as in eq.3.1.

$$B = \mu_r \mu_0 H + B_r \tag{3.1}$$

where B is the magnetic flux density, μ_0 is the permittivity of free space, μ is the relative permittivity and B_r is the remanent flux density. This method models the magnets by generalising the relation in eq.3.1. Modelling using remanent flux density has the possibility to include effects of demagnetisation in case an external field is applied in a direction reverse to the present direction of magnetizing current [7].

To define the magnetic vector at the edges of the border, the periodic conditions are set where 'antiperiodicity' is chosen as at the destination edge, the magnitude of the vector remains the same but the direction reverses [40]. This is illustrated in fig.3.11 and fig.3.12
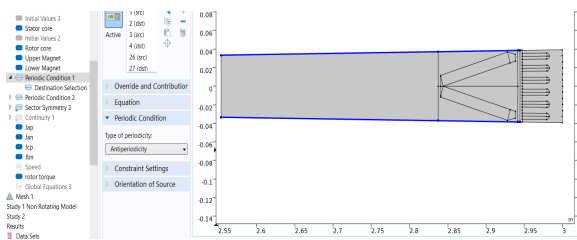
Figure 3.10: Defining Vector

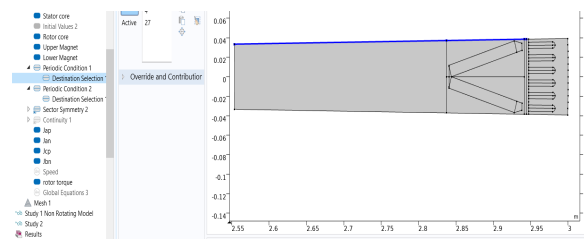Figure 3.11: Selection of Boundary Condition 1

Figure 3.12: Selection of Boundary Condition 2

3.2.3. Step 3: Meshing the geometry

Choosing default 'physics-controlled' meshing is a quick way to mesh the geometry as an automatic unstructured tetrahedral mesh is created which adapts as per the model's settings. However a drawback to this setting is that too many elements are created which may slow down the solving time. In that case, customising the mesh or using user defined mesh reduces the number of elements that leads to a lesser computation time [6]. However with respect to the model used in the thesis, 'physics controlled' mesh of 'finer' size is found to have sufficiently fast computation time.
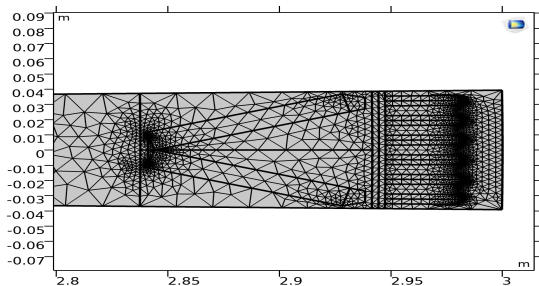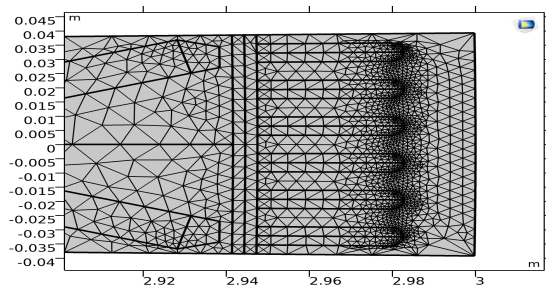

Figure 3.13: Geometry after meshing

Figure 3.14: Meshing at air gap and stator slots

3.2.4. Step 4: Solving: Simulation of the model

In the magnetic circuit model used, as discussed in section 2.1.2, the bridge is assumed to be saturated. While simulating the model, the value of B_{sat} which is a property of the material used is determined as shown in fig.3.15. Where k is the ratio of length to width of magnet, θ_{mag} is the angle between the magnets. First, values of k, θ_{mag} and B_{sat} are assumed as starting values. They are iteratively adjusted until the exact values are obtained.

3.2.5. Step 5: Analysis of the model

Analysis of the model primarily involves deriving the desired parameters from the solved FEM model done partly in COMSOL and MATLAB with Livelink to interface between them. The characteristics of
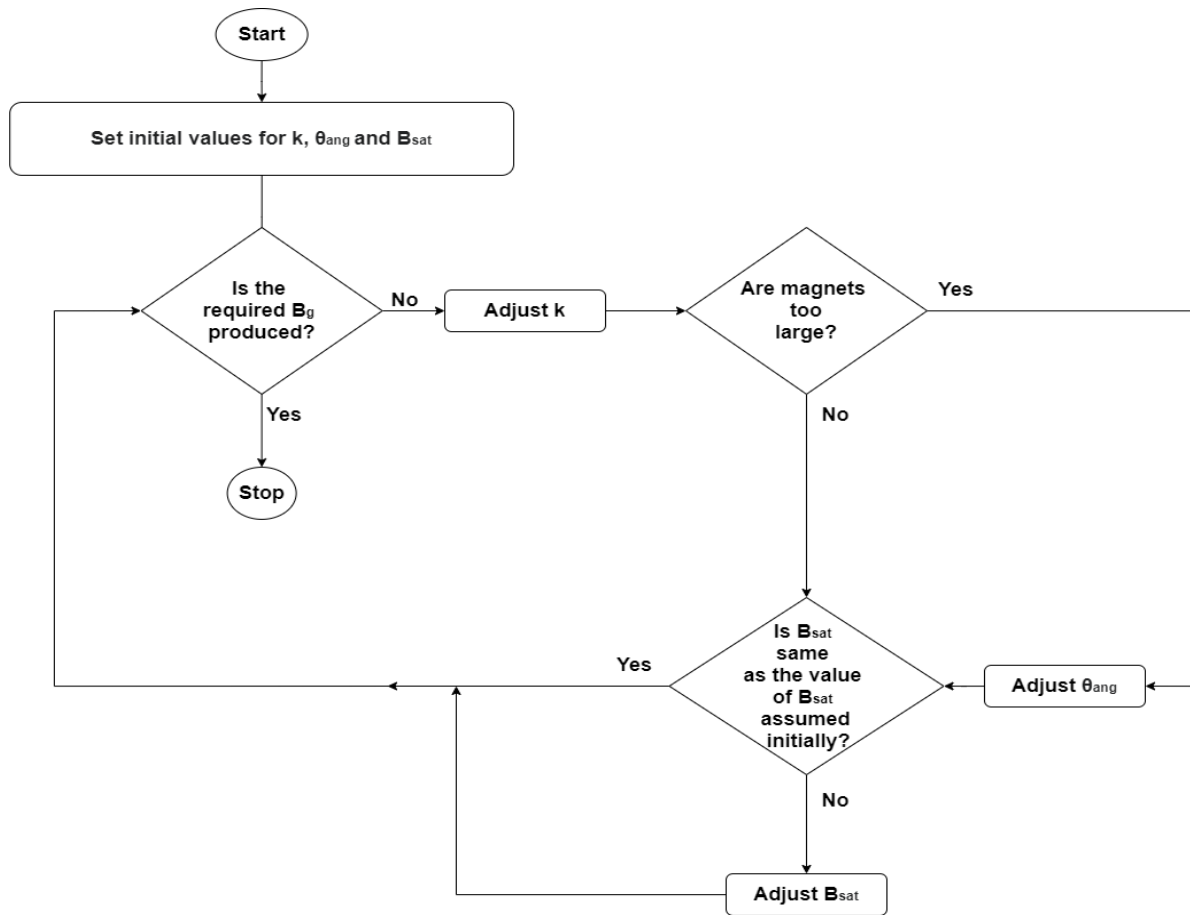
Figure 3.15: Flowchart: finding exact value of B_{sat}, k and θ_{mag}

the machine such as the air gap flux density, three phase flux linkages, FFT of induced EMF, inductance and torque calculations are calculated and validated. This is discussed in detail in section 3.3.

3.3. Analysis and Validation of the FEM Model

After simulating the model as a stationary machine, the solution is given in fig.3.16.
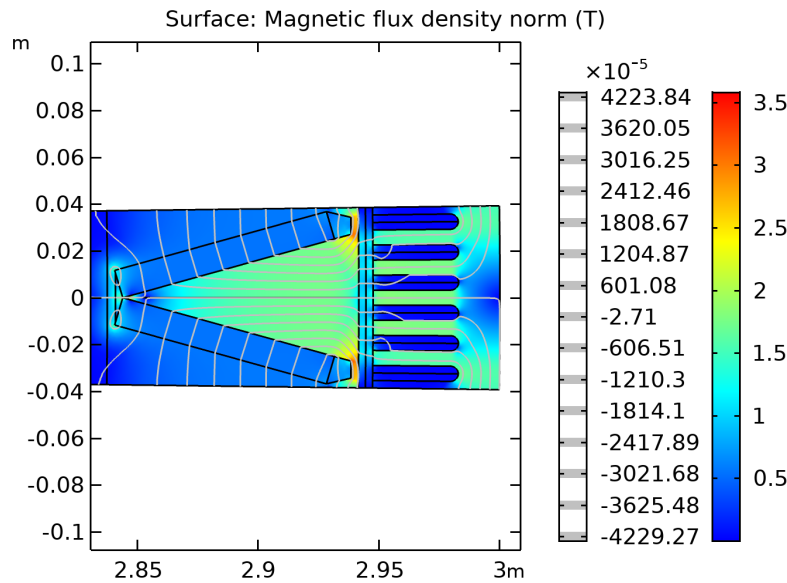
Figure 3.16: Magnetic Flux Density and Vector Potential
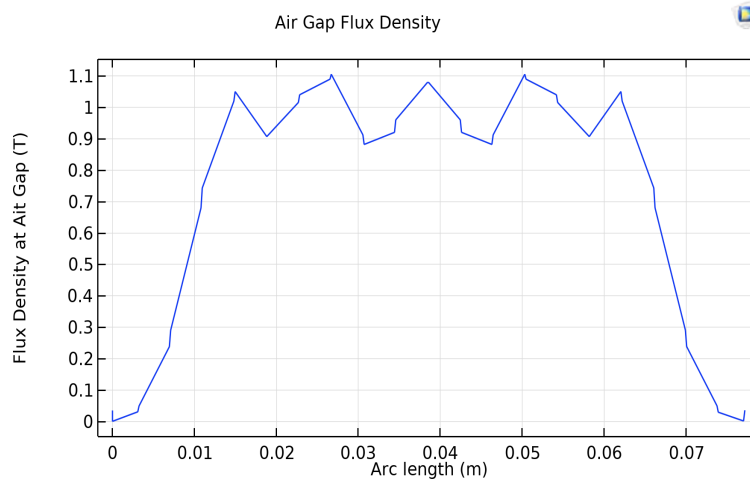
Figure 3.17: Flux Density at the Air gap

The magnetic flux density in fig.3.17 is very close to the expected value. The minute reduction can be understood on closely examining the flux lines through air gap as in fig.3.18, where it can be seen that flux lines towards the end of the magnet are not crossing the air gap.

Since the FEM model produces a value of magnetic flux density close to 0.9T at air gap as the analytical model, the model is validated.

3.3.1. Flux Linkages

From eq. 2.59 the flux linkages are obtained
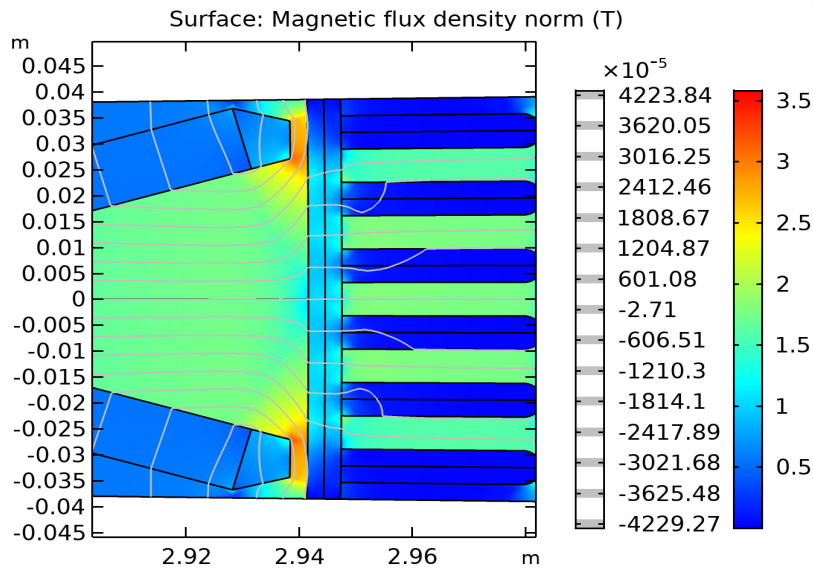
Figure 3.18: Magnetic Flux Density at the air gap and surrounding region
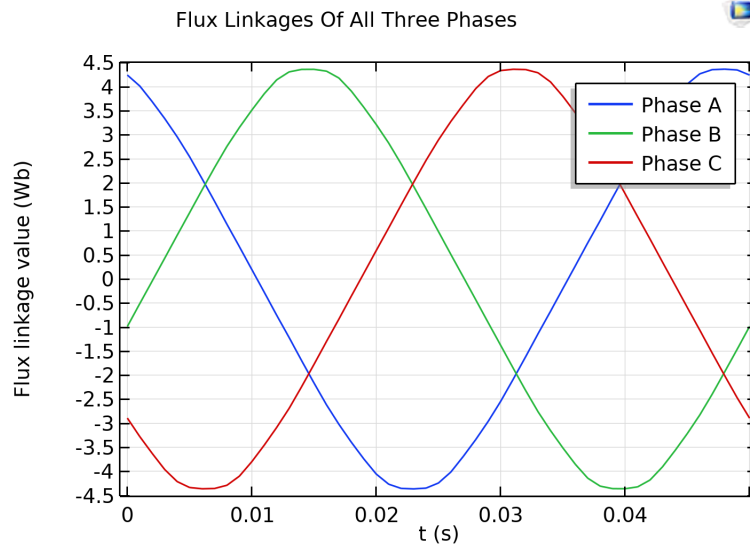
Figure 3.19: Three phase Flux Linkages
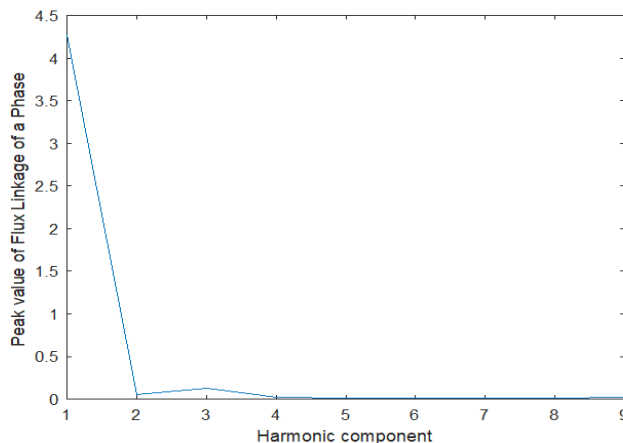
Figure 3.20: FFT of phase A flux linkages

From eq. 2.60, the peak phase value of analytical flux linkages is 4.3137 Wb whereas the peak phase value of FEM flux linkages 4.2679 Wb. This is shown in table 3.7.

Parameter	Value
Analytical $\lambda_{ph-peak}$	4.3137 Wb
FEM $\lambda_{ph-peak}$	4.2679 Wb
Error(%)	1.062

Table 3.7: Validation of Flux linkages

3.3.2. Induced EMF
From eq. 2.57 the Induced EMF is obtained.
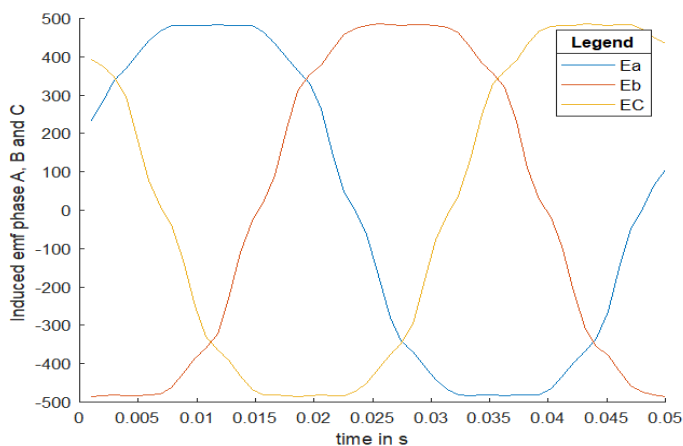
Figure 3.21: Induced EMF of all three phases

The peak value of phase voltage is obtained by Fast Fourier Transform (FFT) as shown in fig. 3.22.

Validation of Induced EMF:
The percentage error is calculated as shown in table 3.8.

Figure 3.22: FFT of Induced EMF in a phase

Parameter	Value
Analytical $E_{ph-peak}$	542.07 V
FEM $E_{ph-peak}$	536.84 V
Error(%)	0.964

Table 3.8: Validation of Induced EMF

3.3.3. Inductance

Inductances from the FEM model were using equations in chapter 2, section 2.3.3. Analytical inductances were calculated using the equations in chapter 2, section 2.1.5. There is a considerable amount

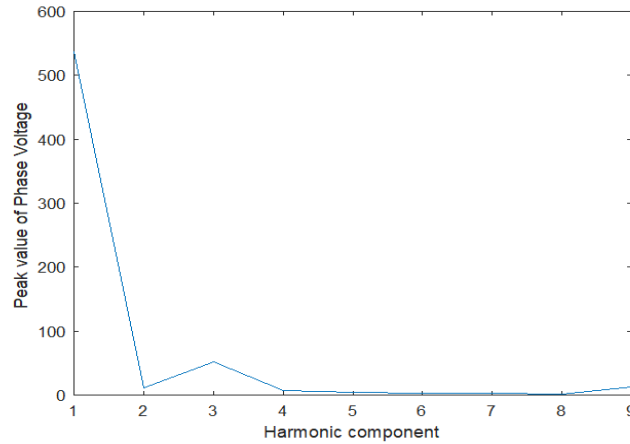| Model/Parameter	$L_d(10^{-4}H)$	$L_q(10^{-4}H)$	Ratio : L_q/L_d
Analytical	7.507	8.935	1.19
FEM	2.988	7.235	2.421
Error %	60.20	19.02	103.44

Table 3.9: Validation of Inductance

of difference in the values of inductance - specifically in d axis. This could be because of the effect of saturation. In case of magnetic saturation, the inductances of machine no longer vary linearly with respect to the current [28].

3.3.4. Simulation and validation of torque

Amplitude invariant Park transform is used to convert the current from ABC to dq0 format. For this reason, it is necessary to ensure that the flux linkages are aligned correctly i.e. phase A is aligned with d axis. Else the displacement δ in eq. 2.62 is included in Park Transform to align both the axes. Enlarging figure 3.19 near a portion of minute displacement

The value of displacement is calculated and applied correctly in the Park Transform formula.

As seen in fig. 3.24, the value of λ_q is zero; implying that the displacement is correct.

Axial torque is the torque computed by COMSOL. This method used surface integration where Maxwell's stresses are integrated over the whole outer boundary of the selected domain. The drawback of this method is that it is sensitive to mesh size where a finer mesh would produce better results [39]. this method is based on surface integration; the computed force is sensitive to mesh size. When using this method, it is important to always perform a mesh refinement study to correctly compute the force or torque. Both Axial and Arkkio's torque produced are lower than the desired value of torque. Also, the shape of the axial torque calculated by COMSOL doesn't closely follow the Arkkio's torque that is supposed to be produced as per the geometry.

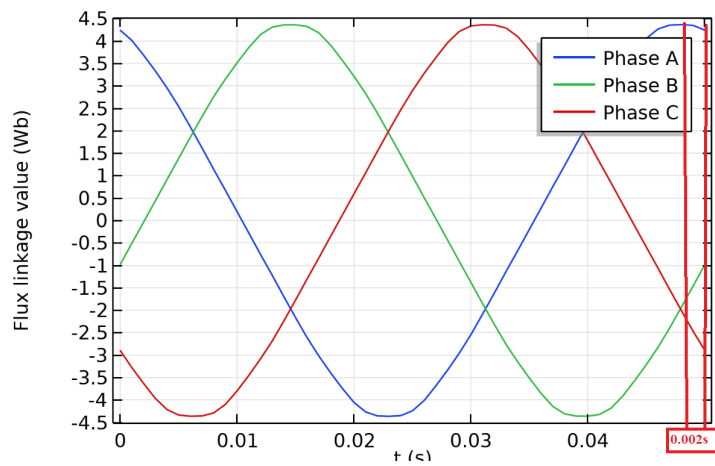Since Arkkio's method of obtaining Torque completely depends upon the geometry, this implies that that

Figure 3.23: Enlarging portion near flux linkage displacement
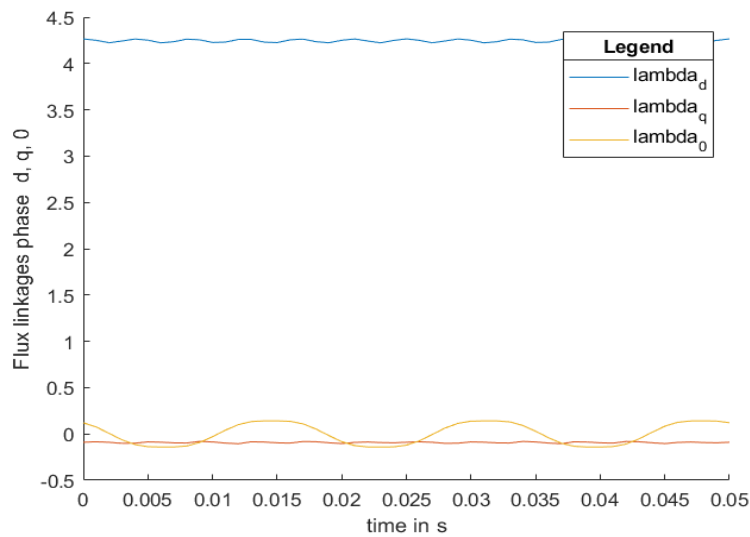

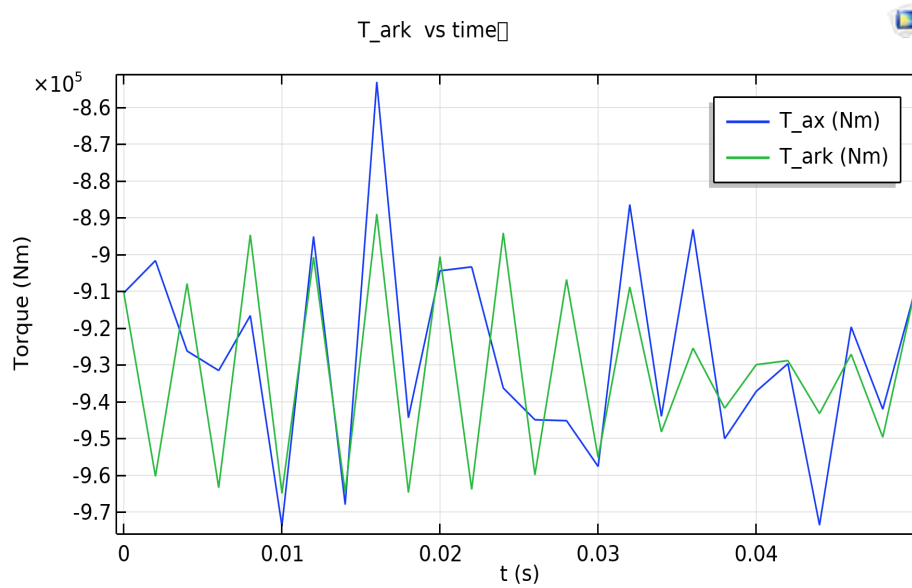Figure 3.24: Flux Linkages of d,q,0 after Park Transform at no load

Figure 3.25: Simulation of torque

that the geometry of the model is not sufficient enough to produce the desired Torque. This is probably because of the fact that the main dimensions of the machine are obtained from the sizing equation. However, sizing equation only gives an estimate of the dimension and not the exact dimensions. This reduction is in consistence with the lower than desired flux linkages and induced EMF.

Validation of Torque

Parameter	Value
Desired T_{mech}	$9.549*(10^5)Nm$
Produced T_{mech}	$9.3*(10^5)Nm$
Error(%)	2.616

Table 3.10: Validation of Torque

As shown in table 3.10, the produced torque is close to the desired torque with an error of 2.616%.

3.3.5. Performance calculation
The performance of this machine are calculated based on the methodology discussed in chapter 2 section 2.4.5.

Parameter	Value
Total Efficiency (%)	91.647
Total Volume (m^3)	14.765
Mag. Wgt. per pole pair (kg)	17.34

Table 3.11: Performance of the initial model

3.3.6. Observations and Remarks
A major advantage of the initial design is its small volume. However, this design has many drawbacks such as lower efficiency, high magnet weights and mismatch in values of inductance because of saturation. It is necessary to use a multi-objective algorithm to optimise the model considering total efficiency, total volume and magnet weight per pole pair as the objectives. To optimise the machine, the design parameters have to be identified.

Sr. no.	Characteristic/Performance	Value
1	$E_{line-rms}$	663.9 V
2	i_{ph-rms}	869.64 A
3	N_{series}	160
4	n_{pp}	3
5	L_d	$2.988*10^{-4}H$
6	L_q	$7.235*10^{-4}H$
7	Torque	$9.3*(10^5)Nm$
8	Total efficiency	91.647%
9	Total volume	14.765 m^3
10	Magnet weight per pole pair	17.34 kg

Table 3.12: Total summary: characteristics and performance of initial model

Identification of Design Parameters

Stator outer radius r_{so}, axial length l and ratio of length to width of magnet (k) are chosen as three design parameters. The remaining design parameters are identified based on the influence of these parameters from an existing study on IPM machines [12] which are summarised next.

- **Stator inner diameter:** A larger stator diameter elevates minimum flux density in PM and decreases copper loss. However this comes with drawbacks such as increased torque ripple and higher material cost. In this thesis, k_{si} which is the ratio of stator inner radius to stator outer radius is used as one of the design parameters.

- **Air gap length h_g:**

  A larger air gap results in lower core loss and reduced torque ripple. However this will increase the material cost, copper loss and decrease the minimum flux density of PM.

- **Stator tooth width k_{wt}:**

  A thicker tooth width decreases copper loss, elevates magnetic flux density and reduces torque ripple. But core loss as well as cost of material increases.

- **Magnet width h_m:**

  A thicker magnet reduces copper loss and increases the flux density of PM. The core losses depend upon h_m in case of saturation.

- **Pole arc size α:**

  A larger α implies reduced cost, losses and torque ripple. But the extent of this depends upon saturation.

- **Yoke depth y_{thick}:**

  A deeper yoke depth reduces core and copper losses as well as elevates flux density of magnet. However, the material cost increases with depth. This has an exactly opposite effect to that of the slot depth d_s. For optimisation d_s is used as a design variable.

3.4. Summary

In this chapter, the design of the initial model is discussed in detail. The design begins with the sizing of the machine. Next comes the rotor design where the dimensions of magnet are obtained after solving the magnet circuit. This is followed by the design of stator which consists of winding design, calculation of number of parallel path as well as the area of slot. Next part consists of the FEM model where the geometry, physics, meshing and simulation are described in detail. The final part consists of analysis where parameters such as flux linkages, induced EMF, inductance and torque are calculated and validated. Then the performance of the machine is evaluated where the efficiency, volume and magnet weight are calculated. Finally the design parameters for optimisation are selected.

<div align="right">4</div>
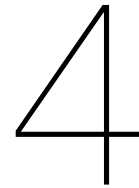
Optimisation by using multi-objective Genetic Algorithm (GA)

4.1. Complete flow chart of multi-objective GA

Fig.4.1 shows the complete flow chart of multi-objective GA. However, this algorithm is time consuming when using Lagrange's multipliers directly and difficult to proceed while trying to find the minimum current from MTPA method. Hence it is simplified for faster compilation.
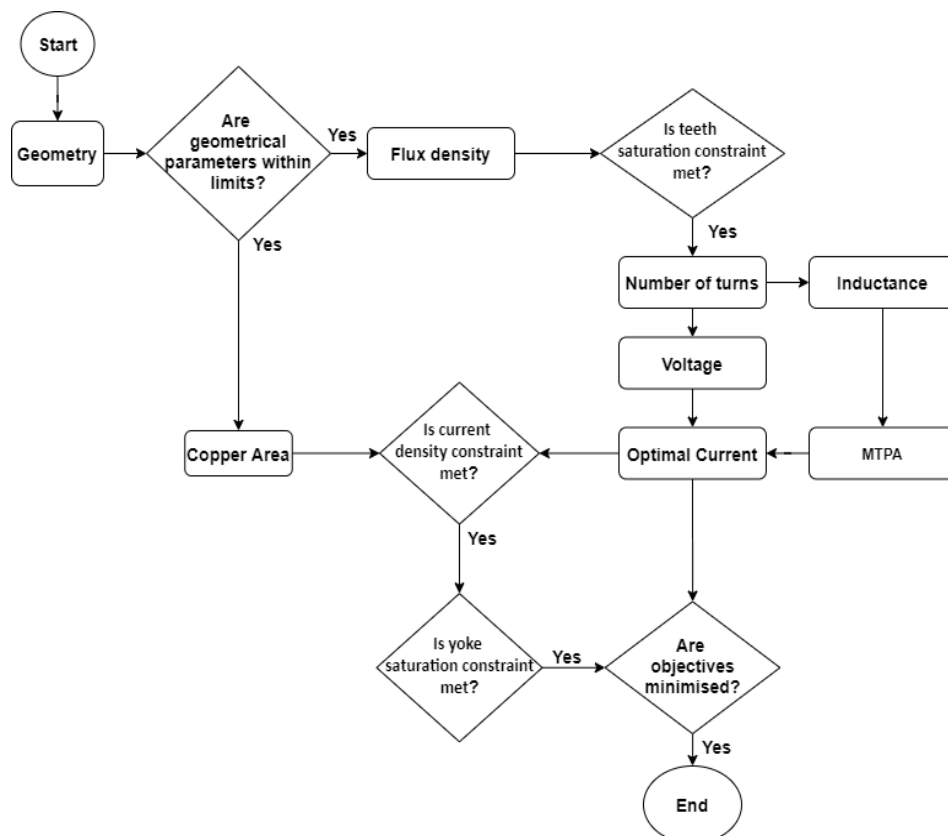

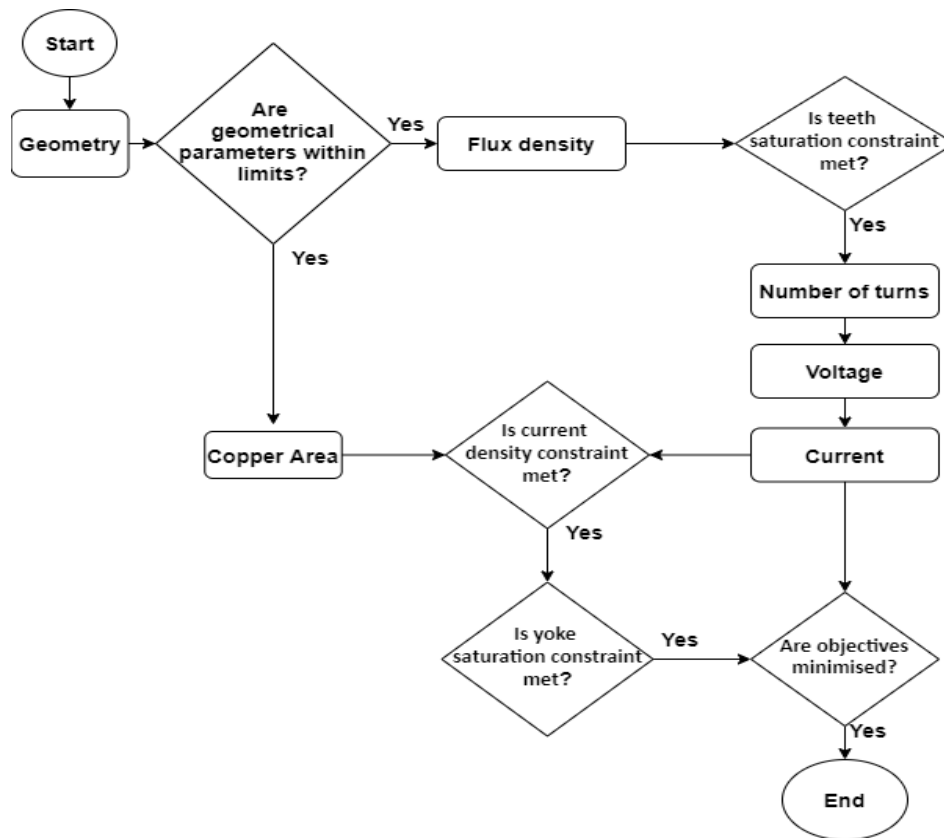Figure 4.1: Complete flow chart of multi-objective GA

Figure 4.2: Simplified Flow Chart of multi-objective GA

4.2. Simplified Flow Chart

Fig.4.2 shows a simplified flow chart where the optimal current is not used for simulation. Though this algorithm has a faster compilation time, this has a drawback of being 'over designed'. This is because the minimum current needed to run the machine is not obtained from the simplified algorithm.

4.3. Pareto Solutions

In the algorithm employed, cross-over is not varied because of the complications associated with it. Apart from varying population size and mutation rate - the maximum generations and maximum stall generations are two features used in the algorithm. 'MaxGenerations' option determines the maximum number of generations the GA takes. Higher the number of 'MaxGenerations', the more accurate the result becomes. 'MaxStallGenerations' determines the number of steps GA takes to check whether the algorithm is making any progress. Increasing this makes GA look further just to ensure that progress is being made [37].

4.3.1. Total volume vs total losses

Figure 4.3 is the Pareto plot of Volume vs Losses. It can be observed that as loss decreases with increases in volume with the highest efficiency being over 94% at a Volume of 30 m^3. The objective is to choose a trade-off point such that both volume and losses are minimised.

4.3.2. Magnet weight per pole pair vs total losses

Figure 4.4 is the Pareto plot of magnet weight vs losses. It can be observed that losses decrease with increase in magnet weight. This is expected because bigger magnets imply stronger field production. However, magnets are expensive and heavy, hence it is essential to minimise the amount of magnets. The objective is to choose a trade-off such that both losses and magnet weight are minimised. The magnet weight calculated here is for a single pole pair. There are 120 such pole pairs in the machine.
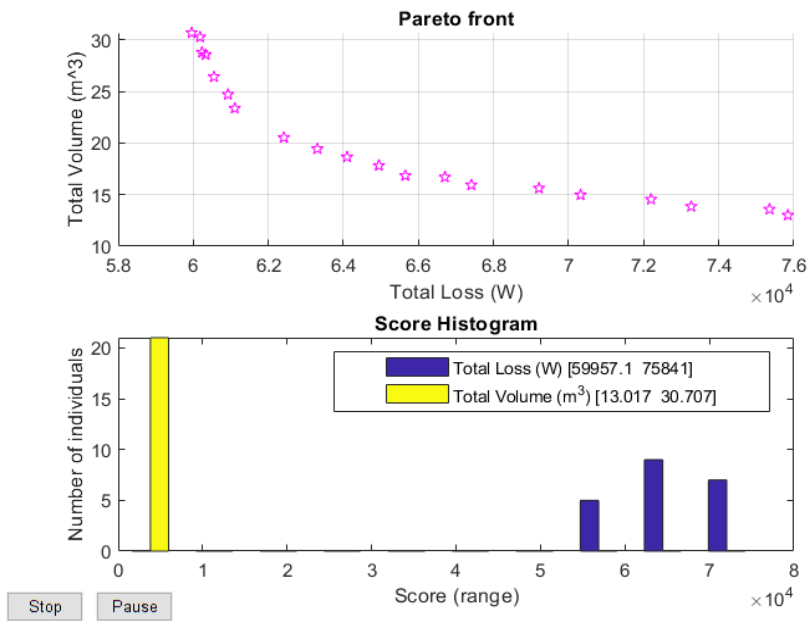
Figure 4.3: Pareto Front : 2 objective : Total volume vs total losses
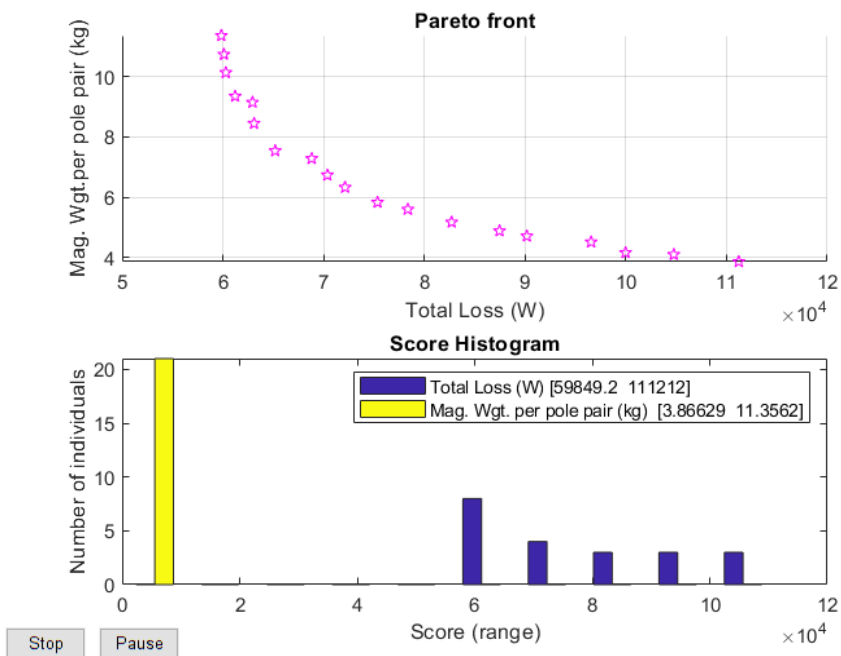
Figure 4.4: Pareto Front : 2 objective : Magnet weight per pole pair vs total losses

4.3.3. Magnet weight per pole pair vs total volume
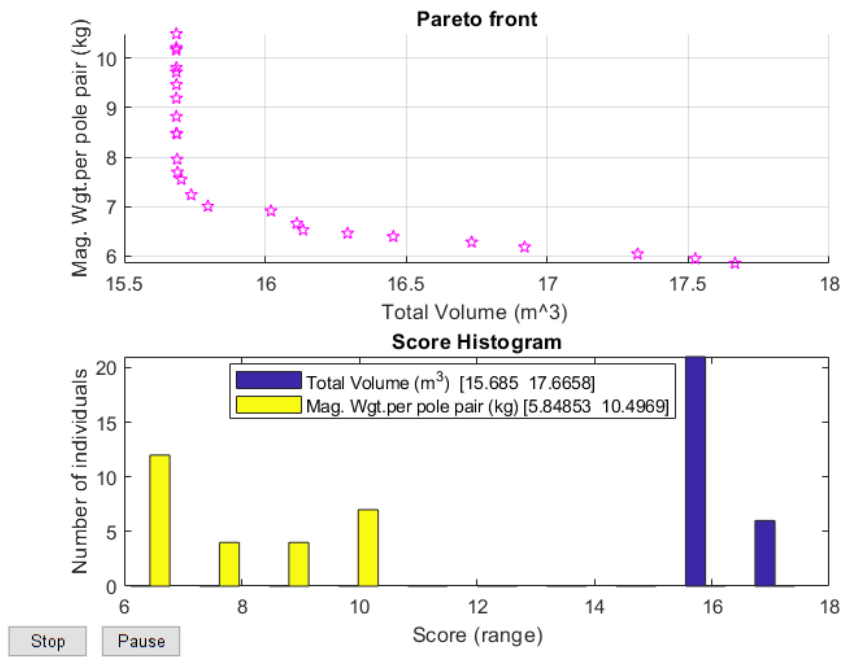
Figure 4.5: Pareto Front : 2 objective : Magnet Weight per pole pair vs Total Volume

Figure 4.5 is the Pareto plot of magnet weight vs volume . It can be observed that within a certain range, the magnet weight decreases with increase in volume.

4.3.4. All three objectives

Figure 4.6: Pareto Front : 3 objective - Total volume vs magnet weight per pole pair vs total loss

Figure 4.6 is the Pareto plot combining all three objectives. However the plot is not dense. It is not having enough solutions at critical points. In order to make the plot more dense and carry out a

refined search; the population size is increased, mutation rate is decreased, the number of generations are increased and the constraint range is made more narrow.

4.3.5. Refined Pareto Plot: All three objectives
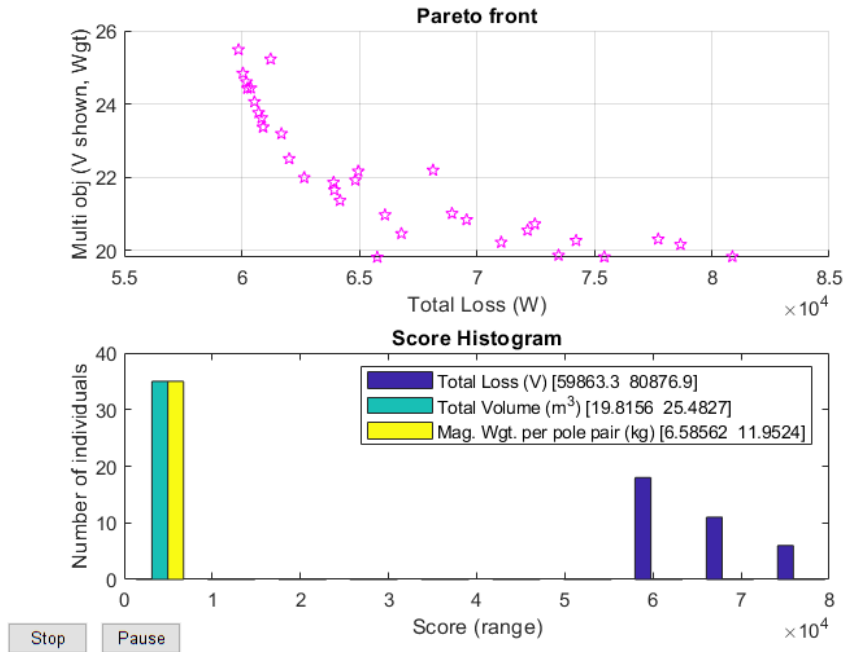
Figure 4.7: Pareto Front : Refined 3 objective - Volume vs Magnet Weight vs Efficiency

Figure 4.7 is a denser Pareto plot combining all three objectives. It can be observed that it contains a large number of solutions at critical points. From this plot, a desired point considering a trade-off between all the three objectives is chosen and then applied to the FEM model. When it comes to trade-off, a higher volume is one factor that can be traded of for better efficiency and lower magnet weights considering that this type of machine is large with most of the magnets and stator slots towards the edge.

4.3.6. Final design parameters and comparison with initial design parameters
In table 4.1, the design parameters of both the initial model and the optimised model are compared.

Design Parameter	Value in Initial Model	Value in Optimised Model
$r_{so}(m)$	3	3.024
k_{si}	0.9825	0.9584
l (m)	0.5222	0.7608
$h_g(mm)$	5.895	3.887
$h_m(mm)$	12.148	9.419
k	7.5	4.253
alpha	0.8	0.809
k_{wt}	0.5	0.461
$d_s(m)$	0.0354	0.059

Table 4.1: Comparison of design parameters

4.4. Summary

This chapter consists of the optimisation procedure using multi-objective GA. The chapter begins with descriptions of both the complete flow chart as well the simplified flow chart where the advantages and disadvantages of both methods are discussed. This is followed by Pareto solutions of total volumes vs total losses, magnet weight per pole pair 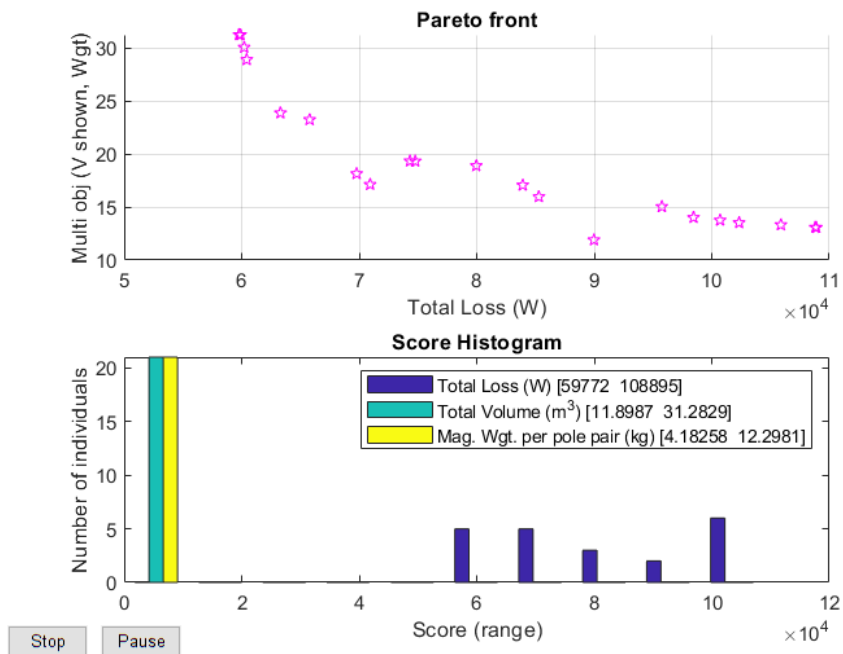vs total losses, magnet weight per pole pair vs total volume, all three objectives and finally the refined Pareto plot from which the final solution is selected. The next chapter of this thesis contains the comparison of final design parameters with initial design parameters.

5

Analysis of Optimised Model

From chapter 4, a selected solution from the Pareto set is applied and an optimised model is obtained. In this chapter, the analysis of the optimised model is discussed in detail. Which is followed by a comparison of the optimised model with the initial model where the geometry, characteristics and performance of both the models are compared.

5.1. Geometry
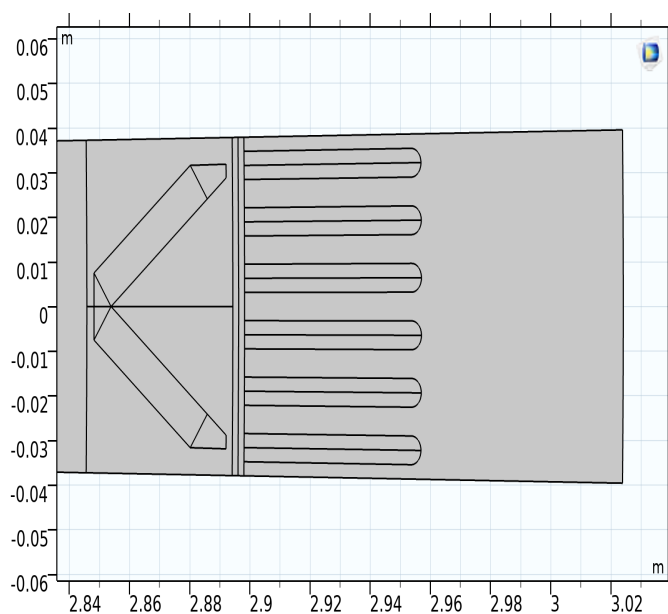
Figure 5.1: Geometry of the Optimised Model

Fig. 5.1 is the geometry of the optimised model. It can be seen that the magnet length is shorter and has higher angle. Also, the yoke dimension is longer compared to the initial design. Additionally, the air gap length is shorter than that of the initial model.

5.2. Analysis and Validation of the FEM Model

5.2.1. Magnetic Flux Density and Vector Potential

After simulating the model as a stationary machine, the obtained solution is shown in fig. 5.2.
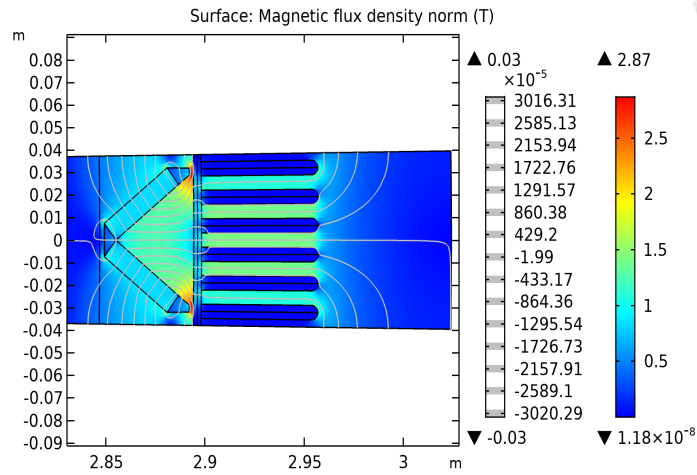
Figure 5.2: Magnetic Flux Density and Vector Potential

5.2.2. Flux Density at Air Gap

After plotting the flux density at the air gap shown in fig. 5.3, it can be seen that the desired value is attained.
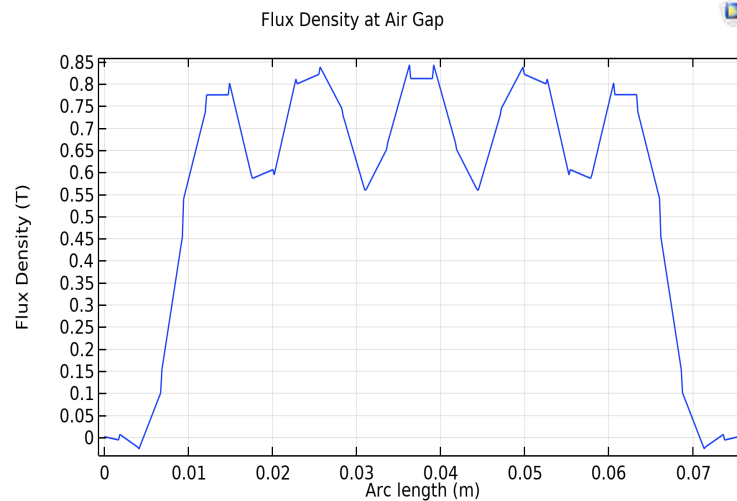
Figure 5.3: Flux Density at the Air gap

A close examination of flux lines near the air gap region is shown in fig. 5.4.

Validation of B_g :

The analytical model was designed so as to produce a magnetic flux density of B_g of 0.67 T, the FEM model also produces the same. Hence, this is validated.

Presently, the algorithm uses one parallel path with 2 conductors per slot. But since the value of voltage is too high, more number of parallel paths are needed. The number of parallel paths is calculated as shown in fig.5.5.

5.2.3. Flux Linkages

To obtain the magnetic flux linkages, the model is simulated for one time period. From eq. 2.59 the flux linkages are obtained. The flux linkages are shown in fig. 5.6.

In order to calculate the peak value, an FFT of the flux linkages is performed as shown in fig. 5.7.
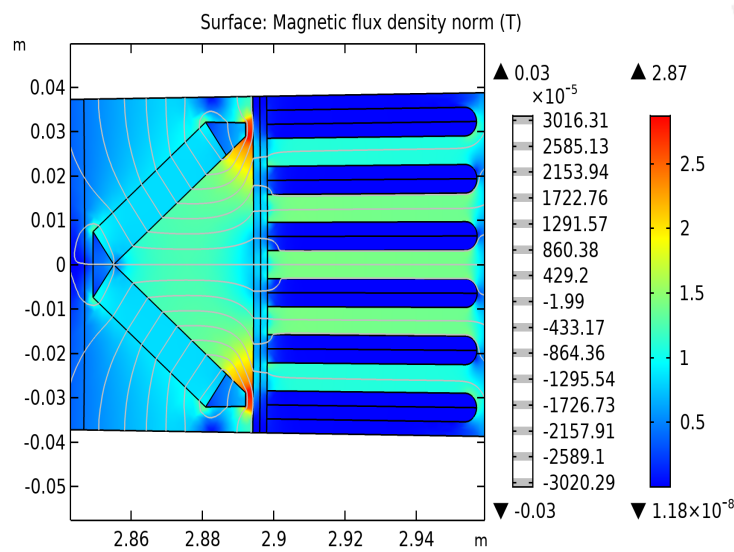
Figure 5.4: Magnetic Flux Density at the air gap and surrounding region
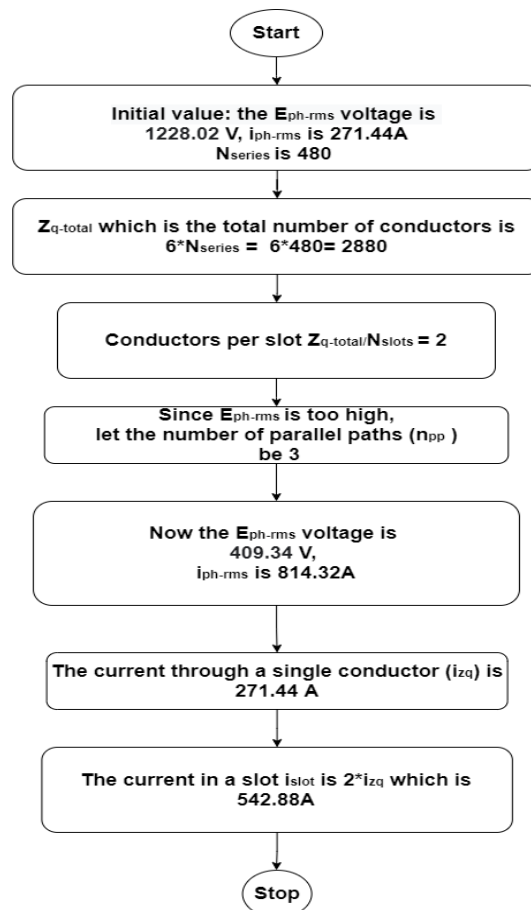
Figure 5.5: Determining parallel paths for optimised model
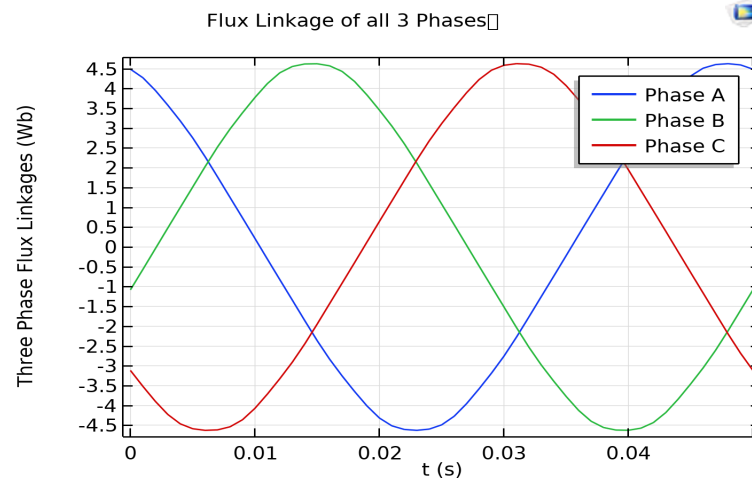
Figure 5.6: Three phase Flux Linkages
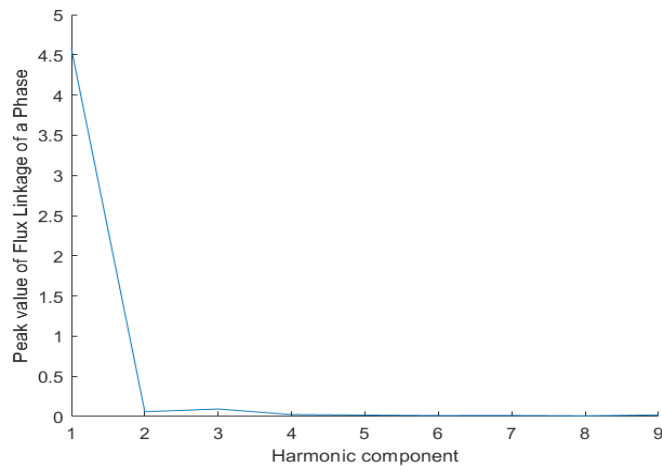
Figure 5.7: FFT of Flux Linkage of a Phase

Validation of Flux linkages:

Using eq. 2.60, the peak phase value of analytical flux linkages is 4.6067 Wb whereas the peak phase value of FEM flux linkages is 4.576 Wb.

The attained value of flux linkages is very close to the desired value. The percentage error is calculated as shown in table 5.1.

Parameter	Value
Analytical $\lambda_{ph-peak}$	4.6067 Wb
FEM $\lambda_{ph-peak}$	4.576 Wb
Error(%)	0.667

Table 5.1: Validation of Flux linkages

5.2.4. Induced EMF

From eq. 2.57 the induced EMF is calculated. The peak value of phase voltage is obtained by Fast Fourier Transform (FFT) as shown in fig. 5.9.
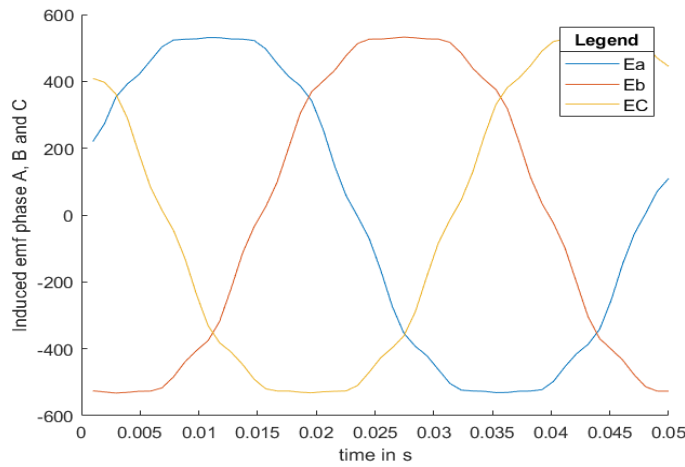
Figure 5.8: Induced EMF of all three phases
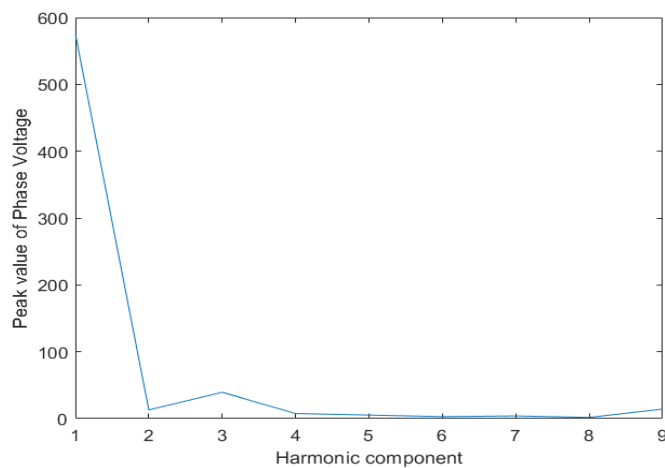
Figure 5.9: FFT of Induced EMF in a phase

Validation of Induced EMF:
The percentage error is calculated in table 5.2.

Parameter	Value
Analytical $E_{ph-peak}$	578.89 V
FEM $E_{ph-peak}$	575.382 V
Error(%)	0.606

Table 5.2: Validation of Induced EMF

5.2.5. Inductance
Inductances from the FEM model were using equations in chapter 2, section 2.3.3. Analytical inductances were calculated using the equations in chapter 2, section 2.1.5.

Model/Parameter	$L_d (10^{-3}H)$	$L_q (10^{-3}H)$	Ratio : L_q/L_d
Analytical	1.3	2	1.538
FEM	1.5	2.08	1.3866
Error %	15.38	4	9.844

Table 5.3: Validation of inductances

There is not much difference in the values of inductance. The percentage error in inductance is very low compared to relatively large difference in the first model.

5.2.6. Simulation and validation of torque
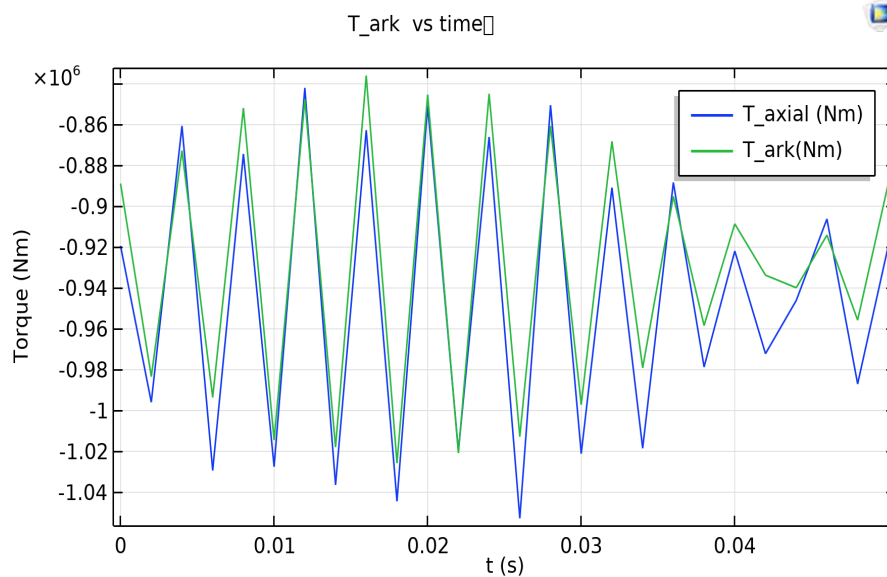
Figure 5.10: Torque Simulation

It can be observed from figure 5.10 that the torque obtained is very close to the desired torque. Also both - the axial torque as well as the Arkkio's torque align well with each other. The percentage error between the desired torque and the actual torque produced is very low as shown in table 5.4.

5.2.7. Performance calculation
The performance of the optimised model which consists of the efficiency, volume and magnet weight per pole pair is calculated and shown in table 5.5.

Parameter	Value
Desired T_{mech}	$9.549*(10^5)Nm$
Produced T_{mech}	$9.4*(10^5)Nm$
Error(%)	1.5634

Table 5.4: Validation of torque

Parameter	Value
Efficiency (%)	93.61
Total Volume (m^3)	21.859
Mag. Wgt. per pole pair (kg)	8.612

Table 5.5: Performance of the optimised model

Sr. no.	Characteristic/Performance	Value
1	$E_{line-rms}$	708.997 V
2	i_{ph-rms}	814.32 A
3	N_{series}	160
4	n_{pp}	3
5	L_d	$1.5*10^{-3}H$
6	L_q	$2.08*10^{-3}H$
7	Torque	$9.4*(10^5)Nm$
8	Total efficiency	93.61%
9	Total volume	21.859 m^3
10	Magnet weight per pole pair	8.612 kg

Table 5.6: Total summary: characteristics and performance of the optimised model

5.2.8. Comparison of both the models
Comparing Cross Sectional Area near the poles of both models:
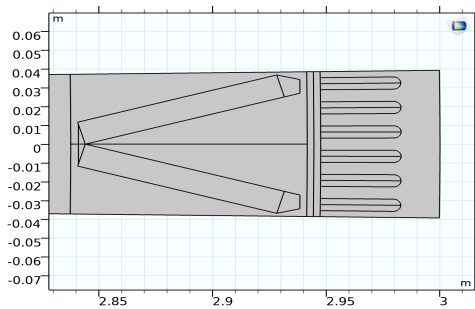
Figure 5.11: Geometry of initial model
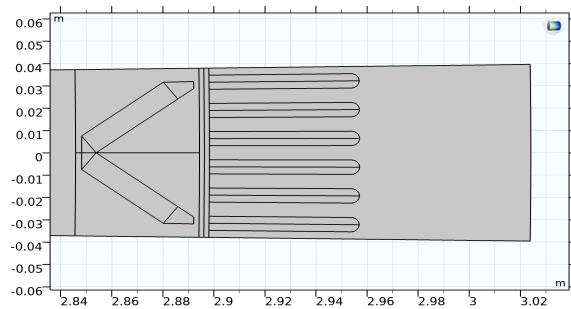
Figure 5.12: Geometry of optimised model

As shown in fig. 5.11 and fig. 5.12, the first model has longer magnets and the slot area is smaller than the magnet area. Also, the yoke is thinner. The air gap is wide. The second model is better when the magnet size, slot area, yoke thickness and air gap are taken into account.

Comparison of torque of both models:
Using fig. 5.13 and fig. 5.14, the torque produced by the initial model and the optimised model can be compared. It can be seen that in the first model, the electromagnetic torque does not smoothly follow the Arkkio's Torque lines. Whereas in case of the optimised model, this problem does not occur. Also the value of the obtained torque is closer to the value of desired torque in the optimised model.

Comparison of characteristics of both the models:
The characteristics of both the models are compared and shown in table 5.7.
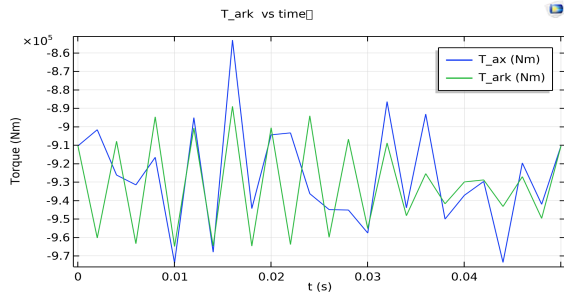
Figure 5.13: Torque of initial model
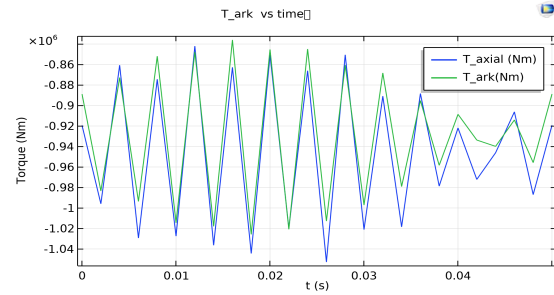
Figure 5.14: Torque of optimised model

Sr. no.	Characteristic	Value in Initial Model	Value in Optimised Model
1	$E_{line-rms}$	663.9 V	708.997 V
2	i_{ph-rms}	869.64 A	814.32 A
4	n_{pp}	3	3
3	N_{total}	480	480
5	Torque	$9.3*(10^5)Nm$	$9.4*(10^5)Nm$

Table 5.7: Summary: Comparison of characteristics of both the models

Comparison of multi-objective performance of both the models:
The multi-objective performance of both the models are compared and shown in table 5.8.

Parameters	Model 1 (First Design)	Model 2 (Optimised Design)
Efficiency (%)	91.647	93.609
Volume (m^3)	14.765	21.859
Magnet Weight per pole pair (kg)	17.34	8.612

Table 5.8: Comparison: multi-objective performance of both the models

5.3. Summary

In this chapter the optimised model is analysed where various parameters like flux linkages, induced EMF, inductance and torque are calculated. In general, the observed values of the optimised model are more closer to the theoretical values on comparison with the initial model, especially in case of the d axis inductance. When geometry is compared, the optimised model has increased yoke thickness and decreased air gap length. Also, the length of magnets is lower. The angle between the magnets is higher. When it comes to torque generation, the axial torque and Arkkio's torque align better and is overall higher in case of the optimised model. When it comes to the performance factors, both the losses as well as the magnet weight are lower in the optimised model. The only drawback being a higher volume. However, when it comes to a trade-off specifically, between magnet weight and volume; for the selected solution, the magnet weight is reduced by half compared to the initial model which is a significant improvement. Overall, the performance of the optimised model is observed to be better than the initial model.

6

Conclusions and Recommendations

This chapter contains a summary of the various conclusions arrived at during the course of this thesis followed by recommendations for future work.

6.1. Conclusions

When it comes to the selection of a suitable machine for a tidal generator; it can be concluded from chapter 1, section 1.1.1 that among the various types of PMSM - embedded magnet PMSM is very suitable for this purpose because such machines are mechanically and magnetically robust. There are several rotor configurations in embedded magnet PMSMs. 'V' type embedded magnet is chosen from existing literature due to their low torque ripple for higher magnitudes of current. However, these magnets have relatively high flux leakage between poles and need more magnet mass. Hence it is necessary to improve the efficiency as well as keep a low magnet weight without increasing the volume of the machine. For this purpose, it becomes necessary to develop a multi-objective optimisation code in order to optimise the machine.

It can be inferred from chapter 2, section 2.4.2 that among GA and PSO, GA is more suitable for optimisation for this particular thesis. Though PSO has inherent multi-objective features and is faster, GA was selected because of its ability to arrive at the correct final result even if some of the intermediate solutions are poor. Also, in PSO, it is hard to define the initial vector. In this thesis, since the model is designed right from the beginning with few constraints, the initial vector may be not close to the final solution. Since the analytical model is used for optimisation, computation time is going to be less. So a slower run time due to GA is not going to be disadvantageous to the overall speed of the optimisation algorithm.

Next a multi-objective GA code is developed after identifying the design parameters from the initial model based on it's influence on the machine performance discussed in chapter 3, section 3.3.6. In chapter 5, section 5.2.8, it can be observed that the optimised model has better efficiency and lower magnet weight at the cost of a slightly higher volume compared to the first model. As explained in chapter 4, section 4.3.5, since the machine is large with most of the magnets and stator slots being towards the edge, volume is one parameter that can be traded off for a better efficiency and magnet weight.

6.2. Recommendations

Some recommendations for future work are:

- **Implementing the algorithm in complete flow chart:**
  Presently, the algorithm in simplified flow chart is implemented. Hence, current higher than the minimum current is used for simulation. Implementing the complete algorithm will enable the usage of optimal current to run the model.

- **Including dimensions of trapezoidal air bubble as a design parameter:**
  Small alterations to the trapezoidal air bubble leads to minor changes in the air gap flux density. Including these dimensions as a design parameter would give a slightly better solution.

- **Varying other geometrical parameters:**
  Changing the shape of slot or using a variable air gap is an option that can be tried in future.

- **Try different slot per pole combination:**
  Different slot per pole combination can be tried to include different geometries for the same topology.

- **Try more options in GA:**
  In GA, as of now; crossover is not altered due to the problems attributed to it. But with more expertise, this can be done. Also developing own codes instead of using MATLAB Optimiser Toolbox would provide better flexibility in dealing with the algorithm.

- **Use spoke type embedded magnet geometry:**
  Spoke type embedded magnet geometry has lesser loss of flux linkages between the poles. This topology could be tried for optimisation.

- **Optimising FEM model with PSO**
  The machine could be optimised by directly using the FEM model. This would take a significantly longer amount of time. PSO would be more suitable for this to reduce the computation time.

A
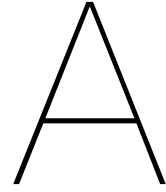
Preliminary Formulae and terminologies

A.1. Preliminary formulae to calculate basic parameters

First some basic parameters have to be determined. The number of poles (P) for a given frequency (f) in Hz and synchronous speed n_s in RPM is determined by:

$$P = \frac{120f}{n_s} \tag{A.1}$$

The number of pole pairs (p) would then be

$$p = \frac{P}{2} \tag{A.2}$$

The mechanical rotation speed in rad/s is given by

$$w_{mech} = \frac{2\pi n_s}{60} \tag{A.3}$$

$$rps = \frac{rpm}{60} \tag{A.4}$$

where rps is the mechanical frequency or the number of rotations per second

$$f_{elec} = rps * p \tag{A.5}$$

where f_{elec} is the electrical frequency

$$T_{elec} = \frac{1}{f_{elec}} \tag{A.6}$$

where T_{elec} is the electrical time period
The torque of a three phase machine is determined using

$$T_{mech} = \frac{P_{mech}}{w_{mech}} \tag{A.7}$$

A.2. Lagrange's multiplier method

Lagrange multipliers is a method used for constrained minimisation/maximisation If F(x, y) is a (sufficiently smooth) function in two variables and g(x, y) is another function in two variables, and we define H(x, y, z) := F(x, y) + zg(x, y), and (a, b) is a relative extremum of F subject to g(x, y) = 0, then there is some value z = λ such that [26]

$$\frac{\partial H}{\partial x}\Big|(a, b, \lambda) = \frac{\partial H}{\partial y}\Big|(a, b, \lambda) = \frac{\partial H}{\partial z}\Big|(a, b, \lambda) = 0 \tag{A.8}$$

Smooth Function
A smooth function is a function that has continuous derivatives up to some desired order over some domain. [38]

A.3. Basic terms in Winding Design

Distributed and Concentrated Winding

Concentrated winding is a type of winding distribution in which all the coils belonging to a winding are placed in one slot. In this case, the voltages induced in the coil are in phase and hence the voltages of the windings is the arithmetic sum of individual coil voltages. This means that under one pole, one slot has one coil side. This in in contrast with distributed windings where the coils belonging to a winding are distributed over several slots in space. Distributed windings make better use of stator structure and reduce harmonics [47].
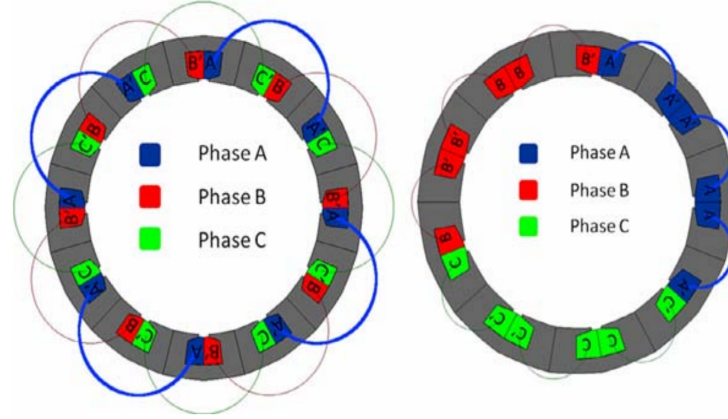
Figure A.1: Distributed and Concentrated Winding [47]

Pole pitch

The distance between the centers of two adjacent poles is known as pole pitch or pole span [47]. The pole pitch is calculated as [42]:

$$\tau_p = \frac{\pi D}{P} \tag{A.9}$$

where τ_p is the pole pitch, D is the stator bore diameter and P is the total number of poles.

Full pitch and short pitch Winding

When coil span is equal to a pole pitch, the winding is called a full pitch winding. If the coil span is less than a pole pitch, the winding is called a short pitch winding. Short pitched winding reduces copper consumption and also significantly reduces certain harmonics. However, flux linkages decrease with short pitch [42] [47].

Steps for winding design are [42]

- First choose the slots/pole number.

- Use winding calculator to obtain various winding configurations.

- Among winding configurations, select that configuration which has the least 5th and 7th harmonics.

A.4. Fourier Series of Even Trapezoidal waveform (Air Gap Flux Density)

For simplification, first B_g is assumed to have a magnitude of 1 for calculation of the integral.

The waveform represents an even periodic function, The generic expression for Fourier series of an even periodic function f(x) for a time period of 2L is given by [32]

$$a_0 = \frac{1}{L} \int_0^L f(x) dx \tag{A.10}$$

$$a_n = \frac{2}{L} \int_0^L f(x) \cos \frac{n\pi x}{L} dx \tag{A.11}$$
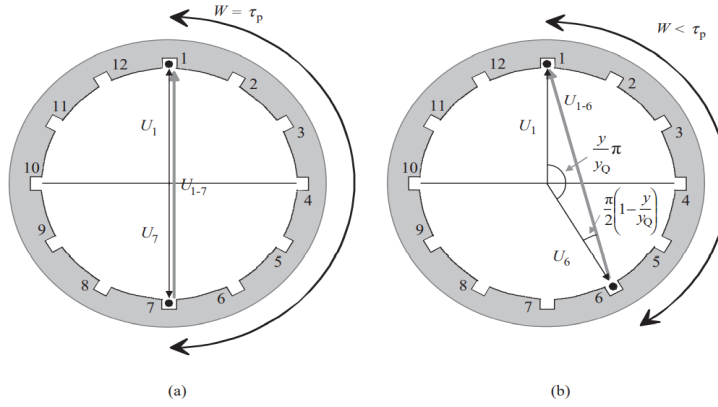
Cross-sectional areas of two machines with 12 slots. The basic differences of (a) a two-pole full-pitch winding and (b) a two-pole short-pitch winding. In the short-pitch winding, the width of a single coil W is less than the pole pitch τ_p or, expressed as the number of slots, the short pitch y is less than a full pitch y_Q. The coil voltage U_{1-6} is lower than U_{1-7}. The short-pitched coil is located on the chord of the periphery, and therefore the winding type is also called a chorded winding. The coil without short pitching is located on the diameter of the machine

Figure A.2: Full pitch and short pitch Winding [42]

$$b_n = 0 \tag{A.12}$$

First, the fundamental component from $(\beta\pi)/2$ to $\pi/2$ is calculated

$$I_1 = \frac{2}{\pi} \int_{\frac{\beta\pi}{2}}^{\frac{\pi}{2}} y(\theta) \cos(\theta) \, d\theta \tag{A.13}$$

Now the expression $y(\theta)$ is the equation of a line which is written as

$$y(\theta) = \frac{1}{\frac{\pi}{2}(\beta - 1)} (\theta - \frac{\pi}{2}) \tag{A.14}$$

Using this expression of $y(\theta)$ in I_1

$$I_1 = \frac{4}{\pi} \frac{1}{\frac{\pi}{2}(\beta - 1)} \int_{\frac{\beta\pi}{2}}^{\frac{\pi}{2}} \theta \cos\theta \, d\theta - \frac{4}{\pi} \frac{1}{\frac{\pi}{2}(\beta - 1)} \frac{\pi}{2} \int_{\frac{\beta\pi}{2}}^{\frac{\pi}{2}} \cos\theta \, d\theta \tag{A.15}$$

Now splitting the integral I_1 into two integrals I_2 and I_3 to simplify calculations such that

$$I_2 = \int_{\frac{\beta\pi}{2}}^{\frac{\pi}{2}} \theta \cos\theta \, d\theta \tag{A.16}$$

$$I_3 = \int_{\frac{\beta\pi}{2}}^{\frac{\pi}{2}} \cos\theta \, d\theta \tag{A.17}$$

After solving the integrals I_2 and I_3 is obtained

$$I_2 = \frac{\pi}{2} - \beta \frac{\pi}{2} \sin\beta \frac{\pi}{2} - \cos\beta \frac{\pi}{2} \tag{A.18}$$

$$I_3 = 1 - \sin\frac{\beta\pi}{2} \tag{A.19}$$

Now substituting solved integrals I_2 and I_3 in I_1

$$I_1 = \frac{4}{\pi} \left[\frac{\cos\beta\frac{\pi}{2} - \frac{\pi}{2}\sin\beta\frac{\pi}{2}(1 - \beta)}{\frac{\pi}{2}(1 - \beta)} \right] \tag{A.20}$$

Next, the fundamental component from 0 to $\frac{\beta\pi}{2}$ is evaluated as

$$I_0 = \frac{4}{\pi} \int_0^{\frac{\beta\pi}{2}} \cos\theta \, d\theta \tag{A.21}$$

On evaluating, the expression I_0 comes to

$$I_0 = \frac{4}{\pi} sin\frac{\beta\pi}{2} \tag{A.22}$$

Combining I_0 and I_1 the fundamental component from o to $\frac{\pi}{2}$ is obtained as

$$I_{total} = \frac{4}{\pi} sin[\frac{(\frac{\pi-\beta\pi}{2})}{(\frac{\pi-\beta\pi}{2})}] \tag{A.23}$$

Considering the magnitude of B_g as such (instead of 1), the fundamental component of the trapezoidal form air gap flux density is

$$Bg_{1-fun} = \frac{4}{\pi} B_g sin[\frac{(\frac{\pi-\beta\pi}{2})}{(\frac{\pi-\beta\pi}{2})}] \tag{A.24}$$

B

Datasheet of materials used

ARNOLD
MAGNETIC TECHNOLOGIES

N35EH

Sintered Neodymium-Iron-Boron Magnets

These are also referred to as "Neo" or NdFeB magnets. They offer a combination of high magnetic output at moderate cost. Please contact Arnold for additional grade information and recommendations for protective coating. Assemblies using these magnets can also be provided.

	Characteristic	Units	min.	nominal	max.
Magnetic Properties	**Br**, Residual Induction	Gauss	11,700	12,000	12,300
		mT	1170	1200	1230
	H$_{cB}$, Coercivity	Oersteds	10,500	11,150	11,800
		kA/m	836	887	939
	H$_{cJ}$, Intrinsic Coercivity	Oersteds	30,000		
		kA/m	2,388		
	BHmax, Maximum Energy Product	MGOe	33	35	37
		kJ/m^3	263	279	295

	Characteristic	Units	C //	C ⊥
Thermal Properties	Reversible Temperature Coefficients [1]			
	of Induction, α(Br)	%/ºC	-0.120	
	of Coercivity, α(Hcj)	%/ºC	-0.420	
	Coefficient of Thermal Expansion [2]	ΔL/L per ºCx10^{-6}	7.5	-0.1
	Thermal Conductivity	W / (m • K)	7.6	
	Specific Heat [3]	J / (kg • K)	460	
	Curie Temperature, Tc	ºC	310	
Other Properties	Flexural Strength	psi	41,300	
		MPa	285	
	Density	g/cm^3	7.5	
	Hardness, Vickers	Hv	620	
	Electrical Resistivity, ρ	μΩ • cm	180	

Notes: (1) Coefficients measured between 20 and   200 ºC
          (2) Between 20 and 200 ºC   (3) Between 20 and 140 ºC

1 kA/m = 12.566 Oe   1 kOe = 79.577 kA/m
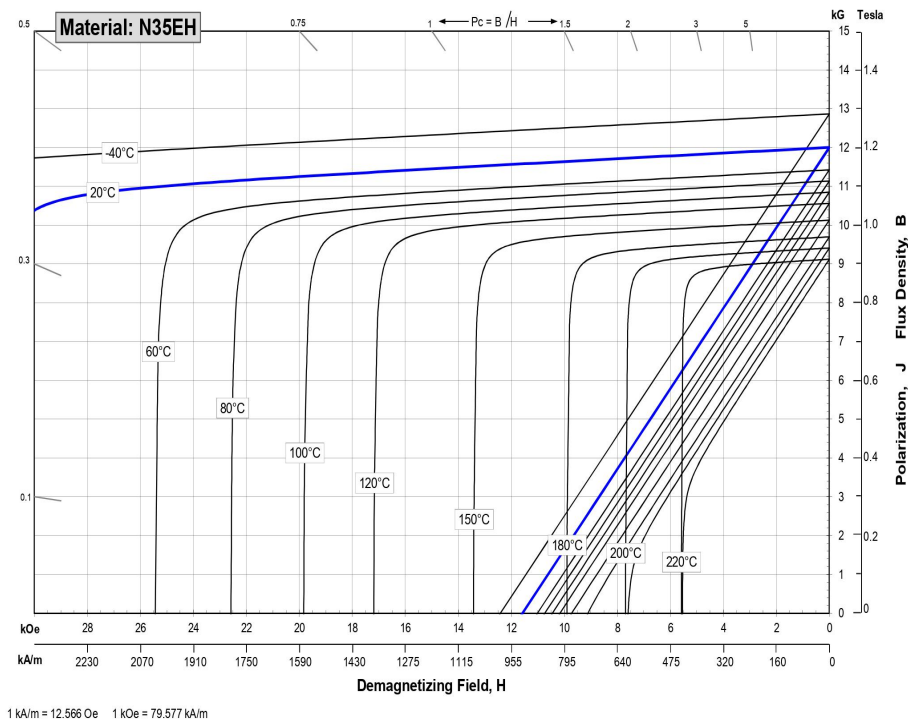
Notes   The material data and demagnetization curves shown above represent typical properties that may vary due to product shape and size.
             Magnets can be supplied thermally stabilized or magnetically calibrated to customer specifications.
             Additional grades are available. Please contact the factory for information.

Figure B.1: Data sheet, Neodymium Iron Boron Magnets material [52].

NONORIENTED ELECTRICAL STEELS

MECHANICAL AND MAGNETIC PROPERTIES

Empirical equations have been developed to describe the typical 60 Hz core loss, 60 Hz exciting power, and D-C magnetizing field strength as a function of induction for each of the more popular grade and gauge combinations of fully processed and semi-processed nonoriented electrical steels. Spread sheets with these equations are available upon request.

TABLE 7 – TYPICAL MECHANICAL AND PHYSICAL PROPERTIES*

Grade	Density gm/cm^3	Yield Strength ksi. (MPa)	Tensile Strength ksi. (MPa)	Elongation % in 2 in. (50 mm)	Rockwell Hardness
DI-MAX M-15 FP	7.65	52 (358)	71 (490)	23	72
DI-MAX M-36 FP	7.70	42 (290)	63 (434)	30	64
DI-MAX M-47 FP	7.75	39 (269)	62 (428)	34	61
DI-MAX M-43 SP **	7.70	50 (345)	70 (483)	32	64
DI-MAX M-47 SP **	7.75	48 (331)	67 (462)	33	62

*Values are typical of data obtained on as-sheared specimens.
**Semi-processed grades have not been quality annealed.

TABLE 8 – TYPICAL D-C MAGNETIC AND ELECTRICAL PROPERTIES

Grade	Electrical Resistivity μΩ·cm	Hysteresis Loss B_{max} = 10 kG J/lb/cycle	Coercive Force B_{max} = 10 kG Oersteds	Maximum Permeability	Saturation Induction KiloGausses
DI-MAX M-15 FP*	50	0.0068	0.41	8000	20.1
DI-MAX M-27 FP*	43	0.0077	0.46	7400	20.5
DI-MAX M-36 FP*	43	0.0085	0.52	6900	20.5
DI-MAX M-43 FP *	43	0.0092	0.57	6500	20.5
DI-MAX M-45 FP *	37	0.0083	0.50	7200	20.8
DI-MAX M-47 FP *	37	0.0094	0.57	6800	20.8
DI-MAX M-43 SP **	43	0.0054	0.30	15000	20.5
DI-MAX M-47 SP **	37	0.0050	0.28	16300	20.8

*Values are typical of data obtained on as-sheared specimens.
**Semi-processed grades have not been quality annealed.

7

Figure B.2: Mechanical and magnetic properties, Non-oriented Electrical Steels [50].

Bibliography

[1] Horizon 2020. *Planning the future of wave and tidal energy*. URL: `https://ec.europa.eu/programmes/horizon2020/en/news/planning-future-wave-and-tidal-energy`. (accessed: 21.12.2020).

[2] Emetor AB. *Electric motor winding calculator*. URL: `https://www.emetor.com/windings/`. (accessed: 30.12.2020).

[3] Emetor AB. *Slot fill factor*. URL: `https://www.emetor.com/glossary/slot-fill-factor/`. (accessed: 4.1.2020).

[4] Zeineb Abdmouleh et al. "Review of optimization techniques applied for the integration of distributed generation from renewable energy sources". In: *Renewable Energy* 113 (May 2017). DOI: `10.1016/j.renene.2017.05.087`.

[5] Zahid Ali. *Permanent Magnet Synchronous Generator*. URL: `https://www.theengineeringknowledge.com/permanent-magnet-synchronous-generator/`. (accessed: 21.12.2020).

[6] COMSOL Blog Caty Fairclough. *Efficiently Mesh Your Model Geometry with Meshing Sequences*. URL: `https://www.comsol.com/blogs/efficiently-mesh-your-model-geometry-with-meshing-sequences/`. (accessed: 2.1.2021).

[7] COMSOL Blog Cesare Tozzo. *Modeling Ferromagnetic Materials in COMSOL Multiphysics*. URL: `https://www.comsol.co.in/blogs/modeling-ferromagnetic-materials-in-comsol-multiphysics/`. (accessed: 2.1.2021).

[8] Our World in Data. *Electricity production by world, Source*. URL: `https://ourworldindata.org/grapher/electricity-prod-source-stacked`. (accessed: 21.12.2020).

[9] Rik De Doncker, Duco Pulle, and André Veltman. *Advanced Electrical Drives: Analysis, Modeling, Control*. Vol. 52. Jan. 2011, pp. 1–443. ISBN: 978-94-007-0179-3. DOI: `10.1007/978-94-007-0181-6`.

[10] Jianning Dong. "Introduction to finite element method for electromagnetics". In: *EE4C05 Electromagnetics Track specification assignments, Delft University of Technology* ().

[11] Y. Duan, R. G. Harley, and T. G. Habetler. "Comparison of Particle Swarm Optimization and Genetic Algorithm in the design of permanent magnet motors". In: *2009 IEEE 6th International Power Electronics and Motion Control Conference*. 2009, pp. 822–825. DOI: `10.1109/IPEMC.2009.5157497`.

[12] A. Fatemi, D. M. Ionel, and N. A. O. Demerdash. "Identification of design rules for interior PM motors with different cooling systems". In: *2015 IEEE International Electric Machines Drives Conference (IEMDC)*. 2015, pp. 1228–1234. DOI: `10.1109/IEMDC.2015.7409218`.

[13] A. Fatemi et al. "Optimal Design of IPM Motors With Different Cooling Systems and Winding Configurations". In: *IEEE Transactions on Industry Applications* 52.4 (2016), pp. 3041–3049. DOI: `10.1109/TIA.2016.2553638`.

[14] Domenico Lahaye Fred Vermolen. "Building Virtual Models in Engineering An Introduction to Finite Elements". In: *Delft Institute for Applied Mathematics* (2011).

[15] J.A. Güemes et al. "Comparative study of PMSM with integer-slot and fractional-slot windings". In: Oct. 2010, pp. 1–6. DOI: `10.1109/ICELMACH.2010.5608202`.

[16] Mounir Hadef et al. "An Inverse Problem Approach for Parameter Estimation of Interior Permanent Magnet Synchronous Motor". In: *Progress In Electromagnetics Research B* 31 (Jan. 2011), pp. 15–28. DOI: `10.2528/PIERB11021202`.

[17] Shoudao Huang et al. "Maximum torque per ampere and flux-weakening control for PMSM based on curve fitting". In: (Sept. 2010). DOI: `10.1109/VPPC.2010.5729024`.

[18] Talal Husseini. *Riding the renewable wave: tidal energy advantages and disadvantages*. URL: `https://www.power-technology.com/features/tidal-energy-advantages-and-disadvantages/`. (accessed: 21.12.2020).

[19] GreenBug Energy Inc. *Types of Turbines*. URL: `https://greenbugenergy.com/get-educated-knowledge/types-of-turbines`. (accessed: 21.12.2020).

[20] K. Ishikawa, W. Kitagawa, and T. Takeshita. "Shape optimization of flux barriers in IPMSM by using polygon model method with GP". In: *2014 International Conference on Electrical Machines (ICEM)*. 2014, pp. 1403–1408. DOI: `10.1109/ICELMACH.2014.6960365`.

[21] Szilard Jagasics and Istvan Vajda. "Comparison of different PMSM rotor configurations". In: (Mar. 2015). DOI: `10.1109/IEVC.2014.7056196`.

[22] Gojko Joksimovic. "A.C. Winding Analysis Using a Winding Function Approach". In: *International Journal of Electrical Engineering Education* 48 (Jan. 2011), pp. 34–52. DOI: `10.7227/IJEEE.48.1.4`.

[23] Voratas Kachitvichyanukul*. "Comparison of Three Evolutionary Algorithms: GA, PSO, and DE". In: *Industrial Engineering Management Systems* 11 (3 2012), pp. 215–223. URL: `http://www.iemsjl.org/journalarticle.php?code=1548`.

[24] K. Kim et al. "Multiobjective Optimal Design for Interior Permanent Magnet Synchronous Motor". In: *IEEE Transactions on Magnetics* 45.3 (2009), pp. 1780–1783. DOI: `10.1109/TMAG.2009.2012820`.

[25] Jere Kolehmainen and Jouni Ikaheimo. "Motors With Buried Magnets for Medium-Speed Applications". In: *Energy Conversion, IEEE Transactions on* 23 (Apr. 2008), pp. 86–91. DOI: `10.1109/TEC.2007.914331`.

[26] *Lagrange Multipliers and Constrained Optimization*. URL: `https://math.berkeley.edu/~scanlon/m16bs04/ln/16b2lec3.pdf`. (accessed: 30.12.2020).

[27] Antti Lehikoinen. *Arkkio's Method for Torque Computation*. URL: `https://www.anttilehikoinen.fi/research-work/arkkios-method-torque-computation/`. (accessed: 30.12.2020).

[28] H. Li, J. Melkebeek, and F. De Belie. "Current Response Based Online Inductance Estimation Method for IPMSM DTC Drives Considering Magnetic Saturation". In: *2018 International Symposium on Power Electronics, Electrical Drives, Automation and Motion (SPEEDAM)*. 2018, pp. 39–44. DOI: `10.1109/SPEEDAM.2018.8445257`.

[29] Peixin Liang et al. "Analytical Calculation of D- and Q-axis Inductance for Interior Permanent Magnet Motors Based on Winding Function Theory". In: *Energies* 9 (July 2016), p. 580. DOI: `10.3390/en9080580`.

[30] Huijuan Liu, Haijiao Zhang, and Jingxiong Zhang. "PM Design of IPMSM using Parameterized Finite Element Model". In: *TELKOMNIKA Indonesian Journal of Electrical Engineering* 11 (July 2013). DOI: `10.11591/telkomnika.v11i12.3745`.

[31] M. Mahmoodabadi, R. Maafi, and Milad Taherkhorsandi. "An Optimal Adaptive Robust PID Controller Subject to Fuzzy Rules and Sliding Modes for MIMO Uncertain Chaotic Systems". In: *Applied Soft Computing* 52 (Sept. 2016). DOI: `10.1016/j.asoc.2016.09.007`.

[32] MATH2065. *Introduction to PDEs*. URL: `https://www.maths.usyd.edu.au/MATH2065/r/Week9Lect3.pdf`. (accessed: 4.1.2021).

[33] MathWorks. *Inverse Park Transform*. URL: `https://nl.mathworks.com/help/physmod/sps/ref/inverseparktransform.html`. (accessed: 30.12.2020).

[34] MathWorks. *Multiobjective Optimization*. URL: `https://nl.mathworks.com/discovery/multiobjective-optimization.html`. (accessed: 31.12.2020).

[35] MathWorks. *Park Transform*. URL: `https://nl.mathworks.com/help/physmod/sps/ref/parktransform.html#mw_8100c286-9c75-471b-8c99-35be662e579a_seealso`. (accessed: 30.12.2020).

[36] MathWorks. *Performing a Multiobjective Optimization Using the Genetic Algorithm*. URL: `https://www.researchgate.net/publication/229748079_Fundamentals_of_Genetic_Algorithms`. (accessed: 31.12.2020).

[37] MathWorks. *Set Maximum Number of Generations and Stall Generations*. URL: `https://nl.mathworks.com/help/gads/setting-the-maximum-number-of-generations.html`. (accessed: 4.1.2021).

[38] Wolfram MathWorld. *Smooth Function*. URL: `https://mathworld.wolfram.com/SmoothFunction.html`. (accessed: 30.12.2020).

[39] COMSOL Blog Nirmal Paudel. *How to Analyze an Induction Motor: A TEAM Benchmark Model*. URL: `https://www.comsol.com/blogs/how-to-analyze-an-induction-motor-a-team-benchmark-model/`. (accessed: 2.1.2021).

[40] *Periodic Condition*. URL: `https://doc.comsol.com/5.5/doc/com.comsol.help.sme/sme_ug_solid.07.69.html`. (accessed: 1.1.2021).

[41] TiPA PROJECT. *Background, Conventional PTO vs TiPA PTO*. URL: `https://www.tipa-h2020.eu/tipa-project/`. (accessed: 28.12.2020).

[42] Juha Pyrhönen, Tapani Jokinen, and Valéria Hrabovcová. *Design of Rotating Electrical Machines*. John Wiley Sons, Ltd, 2008. ISBN: 978-0-470-69516-6 (H/B).

[43] M. N. O. Sadiku. *Principles of electromagnetics*. Oxford University Press, 2009. ISBN: 978-0198099154.

[44] A.K. Sawhney. *A Course in Electrical Machine Design*. Dhanpat Rai Co. (P) Limited, 2016. ISBN: 978-8177001013.

[45] E. Sayed et al. "A Comprehensive Review of Flux Barriers in Interior Permanent Magnet Synchronous Machines". In: *IEEE Access* 7 (2019), pp. 149168–149181. DOI: `10.1109/ACCESS.2019.2947047`.

[46] Noelle Eckley Selin. *Tidal power*. URL: `https://www.britannica.com/science/tidal-power`. (accessed: 21.12.2020).

[47] P. C. Sen. *Principles of electric machines and power electronics*. Wiley, 2013. ISBN: 978-1-118-07887-7.

[48] Alexandre da Silva and Djalma Falcao. "Fundamentals of Genetic Algorithms". In: June 2007, pp. 25–42. ISBN: 9780470225868. DOI: `10.1002/9780470225868.ch2`.

[49] A. Starkey et al. "A comparison of particle swarm optimization and genetic algorithms for a multi-objective Type-2 fuzzy logic based system for the optimal allocation of mobile field engineers". In: *2016 IEEE Congress on Evolutionary Computation (CEC)*. 2016, pp. 5068–5075. DOI: `10.1109/CEC.2016.7748332`.

[50] AK Steel. *Nonoriented Electrical Steels, Mechanical and magnetic properties*. URL: `https://www.aksteel.com/sites/default/files/2018-01/m15-m47201310_Final.pdf`. (accessed: 9.1.2020).

[51] Jianxia Sun et al. "Online MTPA Trajectory Tracking of IPMSM Based on a Novel Torque Control Strategy". In: *Energies* 12 (Aug. 2019), p. 3261. DOI: `10.3390/en12173261`.

[52] ARNOLD MAGNETIC TECHNOLOGIES. *Sintered Neodymium-Iron-Boron Magnets*. URL: `https://www.arnoldmagnetics.com/wp-content/uploads/2017/11/N35EH-151021.pdf`. (accessed: 9.1.2020).

[53] George Todorov and Bozhidar Stoev. "Saturation Effects on the Parameters of Interior Permanent Magnet Synchronous Motors with Different Rotor Configuration". In: *Materials Science Forum* 856 (Feb. 2016), pp. 257–262. DOI: `10.4028/www.scientific.net/MSF.856.257`.

[54] MathWorks File Exchange Víctor Martínez-Cagigal. *Multi-Objective Particle Swarm Optimization (MOPSO)*. URL: `https://nl.mathworks.com/matlabcentral/fileexchange/62074-multi-objective-particle-swarm-optimization-mopso`. (accessed: 31.12.2020).

[55] Faisal Wani, Jianning Dong, and Henk Polinder. "Tidal Turbine Generators". In: *Advances in Modelling and Control of Wind and Hydrogenerators*. Ed. by Amir Ebrahimi. Rijeka: IntechOpen, 2020. Chap. 3. DOI: `10.5772/intechopen.90433`. URL: `https://doi.org/10.5772/intechopen.90433`.